

Climate Impacts of Stratospheric Particle Injection



Simon Driscoll
Linacre College
University of Oxford

A thesis submitted for the degree of
Doctor of Philosophy

2013

Inset dedication.

Insert Acknowledgements.

Chapter 1

Abstract

Geoengineering has attracted large attention over recent years as to being a possible way to ameliorate some of the effects of climate change. One of these proposals, involving injecting sulphate aerosols into the stratosphere in order to cool Earth's temperatures back to pre-industrial levels, has been assessed as one of the leading geoengineering proposals. Despite this, large uncertainties remain, in both the physical and social sciences. Small scale trials of sulphate aerosol injection are not seen as ways to provide large amounts of useful data to inform on the climatic response to stratospheric sulphate aerosol loading (whilst also facing many social and ethical barriers). Large scale trials involving injecting amounts of aerosol more comparable to what would be required to cool the Earth's temperature back to pre-industrial levels are viewed as too risky.

Assessments of the climatic effects of sulphate aerosol geoengineering by the scientific community therefore have largely relied on climate modelling studies. We begin this thesis by reviewing sulphate aerosol geoengineering and the modelling studies that have been conducted to date. We then look to nature's analogue, a large explosive volcanic eruption to assess the accuracy if we were to perform our own geoengineering modelling studies. When a volcano erupts it can inject large amounts of sulphate gas into the stratosphere, which then undergo conversion to form sulphate aerosol, cooling the Earth in a way analogous to sulphate aerosol geoengineering. We assess the climatic response to a volcanic eruption and the current ability of climate models to simulate the observed response to volcanic eruptions. The ability of the climate models submitted to the Coupled Model Intercomparison Project 5 (CMIP5) database is

assessed, with a particular focus on dynamical changes in the Northern Hemisphere winter period. These models fail to capture the observed NH dynamical response following eruptions, which is of concern for the accuracy of geoengineering modeling studies that assess the atmospheric response to sulphate aerosol geoengineering.

We then perform simulations of volcanic eruptions with high-top and low-top configurations of HadGEM2-cc, also changing the distribution of the sulphate aerosol implemented in the model. We find the high-top version of HadGEM2-cc gives a markedly improved and statistically significant different post-volcanic winter dynamical simulation to its low-top counterpart, and that the post-winter dynamical simulation in the high-top model agrees with the observed response following volcanic eruptions. We analyse the mechanisms involved in the dynamical changes and conclude that for a simulation to include the full range of feedbacks of sulphate aerosol geoengineering one must use a high-top model capable of capturing the observed dynamical changes to volcanic eruptions. In accord, we conclude by conducting analysis of simulations of sulphate aerosol geoengineering in the high-top configuration of HadGEM2-cc.

Finally, we summarise the project, and assess future work which involving a large host of projects such as incorporating fully interactive chemistry climate models into modelling of volcanic eruptions and sulphate aerosol geoengineering, the modelled and observed arctic summer sea ice response to volcanic eruptions as verification for the modelling studies assessing the impacts of sulphate aerosol geoengineering on sea ice, the monsoon response to volcanic eruptions, changes in the intertropical convergence zone under hemispherically asymmetric volcanic eruptions, and so on.

Contents

Chapter 2

Introduction and motivation, background literature

Geoengineering, defined as “the deliberate large scale intervention in the Earth’s climate system in order to moderate global warming” (Shepherd et al., 2009), has attracted much attention over recent years as a possible solution to avert dangerous anthropogenic climate change (e.g. Wigley, 2006, Crutzen, 2006). Rasch et al. (2008) point out that the reducing fossil fuel emissions to avoid undesirable impacts from climate change requires transformation of technological systems on scales that are unprecedented, and therefore many suggestions of alternative ways to combat climate change have been proposed (see, e.g., Shepherd et al. (2009) and references therein). Many types of geoengineering methods have been proposed (see Shepherd et al. (2009) for a comprehensive introduction). These fit into two categories: Solar Radiation Management (SRM) techniques and Carbon Dioxide Removal (CDR) techniques.

SRM techniques aim to reduce the global mean temperature of the Earth by changing the earth’s global annual mean energy budget (see figure 1.1). This is achieved by scattering a small fraction of the incoming solar radiation back to space. CDR techniques, on the other hand, aim to reduce the levels of Carbon in the atmosphere by actively removing carbon dioxide from the atmosphere and thus reducing the greenhouse gas radiative forcing. Examples of SRM techniques include increasing the surface reflectivity of the planet through painting roofs or placing reflective materials over large areas of desert, enhancement of marine cloud reflectivity, injecting sulphate aerosols into the lower stratosphere, and placing shields or deflectors in space, whilst

examples of CDR techniques include afforestation, biomass/biofuels with carbon sequestration, biochar, enhanced weathering, and ocean fertilisation (Shepherd et al. (2009)).

As CDR methods reduce the amount of carbon dioxide in the atmosphere, they deal directly with the source of increased radiative forcing and climate change. Therefore, they address other effects of climate change, such as ocean acidity, which SRM techniques cannot address in solely reducing atmospheric temperatures. CDR techniques may therefore seem to be the most appropriate. However, CDR techniques currently act on much slower timescales. The size of industry required, cost and problems with scalability from lab to real world, due to the state of the engineering mean that they are not ready for implementation as a viable alternative to mitigation and adaptation, and in the time taken to develop these technologies sufficient economic and ecological damage may incur (Shepherd et al. (2009)). SRM techniques have therefore generated a substantial amount of focus (Mercer et al. (2011)) and are now being investigated (e.g. Robock (2008), Robock (2009), Kravitz (2011), Ricke et al. (2010), Ricke et al. (2011), Irvine (2011), Anti-Llari (2012)). Some SRM techniques have the advantage over that the technology exists such that they can be implemented to full capacity within a few years. Then, they would have very quick impacts on the climate, being able to reduce global average temperature almost immediately (e.g. Kravitz et al. (2013)), so they possess a certain advantage over CDR methods (Shepherd et al., 2009). They are also much cheaper to implement than CDR technologies (e.g. Shepherd et al. (2009), Goes et al. (2012), Davidson et al. (2012), McCellan et al. (2012)) and so have therefore been raised as a luring alternative to more expensive options of CDR, and also mitigation and adaptation. A number of other possible benefits to SRM techniques have been suggested which have raised interest in them, such as possibly prevent the Earth's climate system from passing some tipping points (Irvine et al. 2010). However, many negatives have also been noted (e.g. Robock et al. (2009)), and uncertainty associated with SRM techniques are high. As has been noted, geoengineering is in its infancy (Gadian et al. (2012)), and there is a need to understand the climate impacts of these schemes before ever being implemented (Shepherd et al. (2009)).

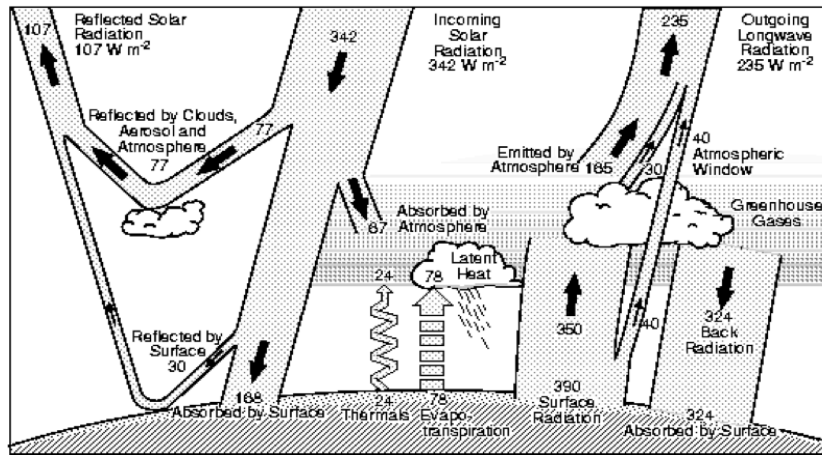


Figure 2.1: The Earth's Global Annual Mean Energy Budget (Kiehl and Trenberth (1997))

Although some voices have either suggested real world experiments to understand the impacts of SRM to be an issue of immediate importance (Victor et al. (2013)), or at least something to strongly consider (Parson and Keith (2013)), many consider this a poor idea (e.g. Robock (2008)). Small perturbations to the climate system would likely require implementation for many years to understand the climate response to this perturbation and whilst progressively larger experiments require less time in order to obtain a clear signal, it is not clear whether any sufficiently large but safe amount of experimentation exists - especially because to know if it is more or less safe one must know to a good extent the effects. Moreover, a number of other social complications and ethical issues exist around the idea of doing real world experiments (e.g. Hamilton et al. (2013)). Therefore, climate modelling studies have been seen as a viable alternative to assessing the impact of sulphate aerosol geoengineering.

Correspondingly, there has been a vastly increasing amount of solar radiation management modelling studies being conducted over the past few years (Mercer et al. (2011)). Early modelling results suggest a mixture of possible benefits and damages from stratospheric aerosol geoengineering. Studies have demonstrated that sulphate aerosol geoengineering is an effective way at cooling global temperatures back to pre-industrial levels (e.g. Robock et al. (2008), Rasch et al. (2008), Jones et al. (2010), Ammann et al. (2010), McCusker et al. (2012), Kravitz et al. (*personal communication/submitted*)). Reducing incoming solar radiation also impacts upon

precipitation, with numerous modelling studies all demonstrating a decrease in precipitation following implementation of sulphate aerosol geoengineering (e.g. Irvine et al. (2009), Ricke et al. (2010), Jones et al. (2010), Ricke et al. (2011), Volodin et al. (2011), MacMynowski et al. (2012), Kravitz et al. (*personal communication/submitted*)) - such a result is understood easily from simple considerations of the surface energy budget analysis and so likely to be robust (Bala et al. (2008)).

The reduced incoming solar radiation has also shown it is possible to affect sea level rise (Moore et al. (2010)). Moore et al. (2010) pointed out that damages from sea level rise from climate change could cost a staggering 10% of projected global gross world product (GWP) in the 2070's, and that geoengineering via sulphate aerosol injection similar to experiencing one Mount Pinatubo eruption every 18 months (injection that would deliver a constant $4Wm^{-2}$ reduction in radiative forcing), could delay sea level rise by 40-80 years when assessing emissions scenarios RCP 3PD, RCP4.5 and RCP8.5 using a simple linear model incorporating effects such as radiative forcing and sea level, but neglecting possibly important feedbacks from ice sheets, and atmospheric dynamics. Irvine et al. (2009) perform simulations in HadCM3L of a sunshade world as an analogy to sulphate aerosol geoengineering, and they conclude that the Greenland Ice sheet can be restored in a four times CO_2 world through the reduction of the solar constant by $57Wm^{-2}$ relative to pre-industrial times (a reduction of 4.2

Sulphate aerosol geoengineering, therefore whilst showing promise at reducing some of the impacts of climate change, are not without bad side effects. Robock et al. (2009), note that would cause a reduction of the ozone in the stratosphere, although Wigley (2006) points out that if stratospheric chlorine levels were to drop as expected then this effect would be reduced relative to ozone loss from stratospheric aerosols today, Tilmes et al. (2008) performed simulations of sulphate aerosol geoengineering using the Whole Atmosphere Chemistry Climate Model 3 estimated that ozone loss from sulphate aerosol geoengineering to be around at least 60 to 80 Dobson Units (DU) for 75% of all winters, with loss being possibly as high as 150 DU under future sulfate aerosol geoengineering scenarios, and they find that the recovery of the

Antarctic ozone hole could be delayed by between 30 and 70 years, indicating large and unintended severe effects from sulphate aerosol geoengineering.

Another major issue for sulphate aerosol geoengineering, is that the reductions in global temperature and precipitation are not expected to be uniform. Ricke et al. (2010) show from simulations of future emissions scenarios that include sulphate aerosol geoengineering, the amount of aerosol needed to return China to within one standard deviation of their pre-industrial temperature in 2070 would not be the same as that for India. Rasch et al. (2008) concluded and concluded that sulphate aerosol geoengineering would not be able to compensate for changes in temperature and rainfall equally across the globe. Irvine et al. (2012) also pointed to tensions due to the possible desired difference in amount of reflected solar radiation for any given country, and particularly that those countries requiring to keep sea level rise to a minimum would require aggressive geoengineering whilst those wishing to keep surface temperature change to a minimum would require much less geoengineering. The non-uniformity of effects has motivated the studies of possible ‘optimisation’ of stratospheric aerosol geoengineering, by implementing aerosol profiles that vary in latitude and in time. The first study on optimisation of stratospheric study was Ban-Weiss and Caldeira (2010). Using the NCAR CAM3.1 model, they first perform a variety of geoengineering simulations with different aerosol profiles. Then they use an optimisation model to predict aerosol profiles most suited to reducing the root mean squared error in zonal average temperature and zonal average precipitation minus evaporation. They conclude that aerosol profiles can be found that result in similar current climate conditions, however the aerosol profiles to minimise temperature and precipitation minus evaporation are different. MacMartin et al. (2012) perform numerous different experiments involving varying solar constant both in latitude and in season. Using HadCM3L they explore the effects of a non-uniform reduction in solar constant on Northern Hemisphere September sea ice extent, precipitation and surface temperature. They conclude that a non-uniform sunshade can achieve benefits such as reducing long term changes in the Northern Hemisphere Sea Ice extent, whilst still being able to reduce impacts globally. They summarise that decisions on geoengineering do not, therefore, need to be reduce to the single decision of the “global

thermostat”.

Despite this, many of these studies should be treated with caution. Often models just impose aerosol, or make the solar constant a variable in latitude and time to represent the effects of a varying aerosol profile. Whether these profiles are at all feasible is not clear. In the following chapter we discuss volcanic influence on climate, and numerous dynamical aspects of the atmosphere, such as the Brewer-Dobson circulation, and the Quasi-Biennial Oscillation, which affect where the aerosol is moved around in the stratosphere (e.g. Aquila et al. (2012)). Also the amount of aerosol that could be put into the stratosphere is unclear. Timmreck et al. (2010), noted a self-limiting effect of supervolcanoes, with the more sulphate injected into the stratosphere, the larger the particles due to larger amounts of coagulation, and therefore more rapid fallout. Similarly, in a modelling study, Hommel and Graf (2010) conclude that sedimentation to due aerosol sizes may act to impose a natural limit on the ability of sulphate aerosols geoengineering proposals to reach their achieved cooling target. These effects are not included in the optimisation studies above.

The effect of geoengineering on the biosphere is also uncertain. Increased levels of diffuse light over scattered light With increasing CO_2 , photosynthesis levels and CO_2 uptake levels (with stabilising temperatures) Govindasamy et al. (2002) saw an increase in Net Primary Productivity (NPP). However, it must be noted that their studies were very simplified. Rasch et al. (2008) note that although ecosystems can survive occasional volcanic eruptions, their future under stratospheric aerosol geoengineering is unclear.

Haywood et al. (2013) note from observations and a small modelling study that asymmetric volcanic eruptions have caused, in part, Sahelian drought by shifting the position of the ITCZ. Aerosol injected as part of a geoengineering method that is lofted around to be hemispherically non-uniform in the stratosphere could have very serious implications for the climate and livelihood of many people. They note that the Sahelian drought of the 1970s-1990s was one of the largest humanitarian disasters of the past 50 years, causing up to 250,000 deaths and creating 10 million refugees. Robock et al. (2009) note that whilst having a general cooling effect and

so delaying sea level rise and so on, geoengineering could have very large and near-immediate effects on African and Asian precipitation, with effects on reducing the Indian monsoon being something noted from modelling studies (Robock et al. (2008)).

Another major problem is that of the termination effect. It is likely that if started geoengineering would need to continue for hundreds, if not thousands of years. This then leaves the possibility that during this time, geoengineering may be stopped. The rapid loss of aerosols from the atmosphere masking the effects of the fossil fuels in the atmosphere is known as the termination effect, and is expected to lead to a rapid increase in temperatures, which is something also confirmed in modelling studies (Jones et al. (*personal communication/in prep*), McCusker et al. (*submitted*)). It is of course, not something that would be chosen, but we may lose the capacity to do continue doing so (e.g. Baum et al. (2012)), and the effects on the climate and ecosystems would be severe.

Acid rain due to increased sulphate aerosols are not thought to be a major risk due to stratospheric aerosol geoengineering - contributing a relatively small amount of aerosol to the total sulphate aerosol budget when the troposphere is also included (Rasch et al. (2008)). Kravitz et al. (2009) performed modelling studies and assessed that the effects of increased acid rain were likely to be too small to negatively affect most ecosystems.

Still, uncertainty remains high. Wunsch et al. (2013) points out the need for more and better observations and better models, as in their view geoengineering proposals must include an understanding of the influence on the climate system which retains memories of disturbances for thousands of year. Given that we have not observed the climate system's variation on all important timescales, they conclude that our understanding of the impacts of such schemes is poor. Robock (*in prep/personal communication*) also point out the need for better observations of volcanic eruptions in order to understand the full effects of geoengineering on the climate system.

A small handful of ways to increase confidence in the results of geoengineering modelling studies have been proposed. The Geoengineering Model Intercomparison Project (GeoMIP, Kravitz et al. (2011)) was created in order to understand the

variation of model responses to precisely the same experiments. With many geo-engineering studies and effects being discussed from both different experiments, and different models, Kravitz et al. (2011) point out that there is arguably a need to have a standardised set of experiments to compare model responses. Jones et al. (2010) also point out the need for many different climate models to assess the impacts of stratospheric aerosol geoengineering before any consideration is given to practical implementation of such proposals. The four GeoMIP experiments, G1-G4, aim to understand the effects of sulphate aerosol geoengineering, increasing the complexity of the experiment from a solar constant reduction in a future emissions pathway, to full implementation of stratospheric aerosol in the model. Modelling groups around the world have been invited to participate in conducting these experiments, and 12 state of the art models have been used to perform these simulations.

Simulations of the G1 experiment, in which models simulate the climate response to an abrupt quadrupling of CO₂ from preindustrial concentrations brought into radiative balance via uniform insolation reduction, show an insolation reduction does largely offset global mean surface temperature increases due to greenhouse gases but, compared to the preindustrial climate, would leave the tropics cooler (-0.30 K) and the poles warmer (+0.81 K) (Kravitz et al. (*in prep/personal communication*)). Annual mean precipitation minus evaporation (PE) anomalies for G1 are less than 0.2 mm day⁻¹ over 92

There may be some other useful ways to gauge possible impacts without model studies. Lunt et al. (2008) note real occurrences in past climate that may be of use to discerning geoengineering impacts. The Cambrian period, 500 million years ago, experienced a reduction in the solar constant of 57 Wm^2 a 4.2% reduction and it is likely that CO₂ concentrations were higher than pre-industrial, so that in terms of gross radiation balance, a geoengineered world could be broadly similar to the Cambrian World. Despite this, climate modelling studies are the most often way to assess possible effects of sulphate aerosol geoengineering.

At all times, one can go further and question the validity of the models themselves - these studies ultimately hinge on the ability of the models themselves. As previously

mentioned there is a natural analogue to geoengineering of the climate with stratospheric sulphate aerosols: volcanic eruptions. Indeed part of the attraction sulphate aerosol geoengineering, is because volcanoes have already injected sulphates into the atmosphere from an eruption, it is possible to assess the effects from these natural analogues and so sulphate aerosol geoengineering, without having to speculate or rely solely on climate models (Rasch et al. (2008)). Wigley (2006) also states the opinion that the Mount Pinatubo eruption of 1991 did not seriously disrupt the climate system, so geoengineering with sulphate aerosols should therefore present minimal climate risks. When the volcano Mount Pinatubo erupted in June 1991, it released about 10 teragrams of sulphur (TgS) into the stratosphere (Stothers [1996], Bluth et al. [1997], Andres and Kasgnoc [1998]). Whilst the Katmai eruption of 1912 was the most explosive eruption, Mt Pinatubo injected the most sulphate into the stratosphere of any volcanic eruption of the 20th Century (Robock, 2003). Correspondingly, incoming solar radiation was reduced, with a radiative forcing peak annual mean value of -2.9 W/m^2 (Wigley, 2006). The aerosol cloud reduced the net flux radiation in the tropics by around $5\text{-}6 \text{ W/m}^2$, and the Earth's globally averaged surface temperature decreased by approximately 0.3°K for two years after the eruption, whilst the lower tropical stratosphere increased by approximately $2\text{-}3 \text{ K}$ because the sulphate aerosol released by volcanoes, as well as reflecting and scattering SW radiation, is also absorbing in the LW Infra-Red and solar near-IR radiation (Stenchikov et al. (2002)). Such a large perturbations caused many effects on the climate system, and in the next chapter we focus on the effects of volcanic eruptions on the climate so as to ultimately assess the reliability of performing a geoengineering modelling study.

It is this view, with geoengineering in focus, that I have first sought to understand the climatic response to a large explosive volcanic eruption, then assessed the modelled response to volcanic eruptions to understand the accuracy of my geoengineering simulations, and finally I return at the end of the thesis to analyse a small number of geongineering simulations.

Chapter 3

Volcanic Eruptions and their effect on climate

3.1 Literature Review

For a volcano to have a significant long-term impact on the climate it must inject a sufficient amount of sulfur containing gases into the stratosphere (?). Sulphate injected into the troposphere will get washed out in a few days, however particles that are injected into the stratosphere can stay up in the atmosphere for one to two years (Cole-Dai, 2010). Once in the stratosphere the sulfate gas undergoes a chemical reaction to produce sulfate aerosol. The e-folding time of the sulfate gas to particle conversion is typically 30-40 days (?). Sulfate aerosol scatters back to space the incoming shortwave radiation (SW) and also absorbs solar near infrared (NIR) radiation and upwelling long wave (LW) radiation from the surface and atmosphere below (???). For a given mass load, the scattering of SW radiation is modulated by the particle size distribution and as the aerosol particle size increases, scattering of incoming SW radiation decreases (?). The decrease in incoming shortwave radiation results in a cooling of Earth's surface (?). The typical e-folding lifetime for tropically injected volcanic aerosols is about 12-14 months (???), and larger particles fall out of the stratosphere faster than smaller particles. However they can have a longer residence time if they are injected into the tropics because of uplifting due to the Brewer-Dobson circulation (Kravitz and Robock (2011), Budyko (1977), Stenchikov et al. (1998)). Figure 3.1 shows some of the basic radiative and chemical effects following a volcano eruption.

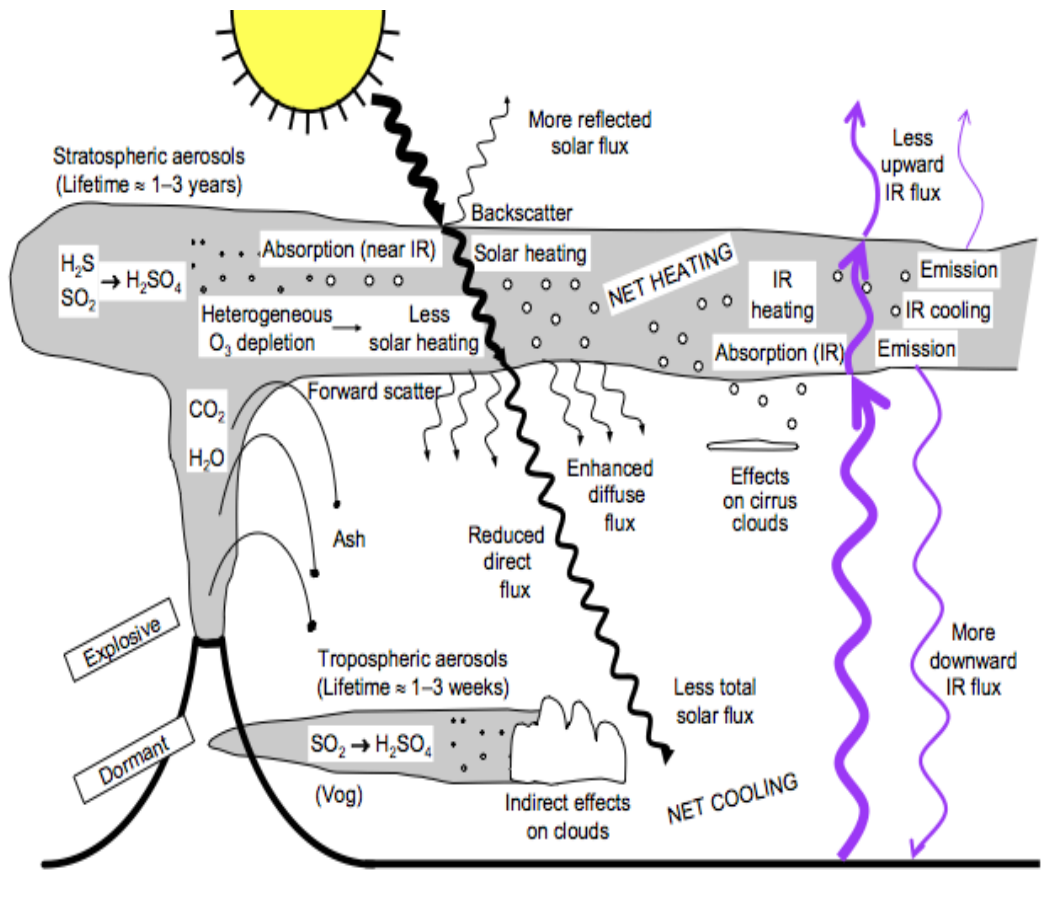


Figure 3.1: Basic radiative and chemical impact of a volcanic eruption on the Atmosphere, from Robock (2000)

Whilst the climate effect of a volcano eruption is very much dependent on latitude (e.g. Fischer et al. (2007), Stenchikov et al. (2006)) and the time of year of the eruption (Kravitz and Robock (2011)), with for example the Kasatochi eruption of August 2008, the largest eruption since Mount Pinatubo in 1991, showing negligible climate effects despite injecting 1.5 Tg of SO_2 in stratosphere (due to injection too late in the year and too high latitude to cause any major effect shortly after eruption, and too low in magnitude and high in latitude to last into spring), and eruptions at different latitudes showing a markedly different dynamical response (Oman et al. (2005), Kravitz and Robock (2011)) the cooling following volcanic eruptions is a generally robust feature.

In contrast to the surface there is heating in the lower stratosphere due to the increase in longwave absorption in the region from the presence of aerosols. Follow-

ing this surface cooling, and lower stratospheric heating, an important dynamical effect occurs (see figure 3.2 for a schematic diagram), which is believed to result in Northern Hemisphere winter surface warming over Eurasia and North America, and cooling over Greenland and the Eastern Mediterranean (e.g. Robock and Mao (1992), Robock (2000), Shindell et al. (2004), Fischer et al. (2007)). The increase in long-wave absorption in the lower stratosphere causes heating as large as 3K in the case of the 1991 Mount Pinatubo eruption (Stenchikov et al. (2002)). The warming of the tropical lower stratosphere creates an anomalous temperature/density gradient between the equator and poles. By thermal wind, this causes a strengthening of the zonal winds, which results in the stratospheric polar vortex strengthening. Moreover, reduced surface temperatures in the tropical regions reduce the meridional surface temperature gradient, which causes a reduction in the Eliassen Palm Flux - essentially, a measure of the eddy flux and momentum flux (Andrews et al. (1987)) - into the vortex, which means that the vortex is less disturbed and thus stronger. Further, chemical reactions which result in Ozone depletion (e.g. Telford et al. (2009)) cool and strengthen the vortex, and the reduced temperatures cause more Ozone depletion, creating a feedback loop. Model simulations have shown that an atmosphere with an intentionally cooler polar stratosphere (without the increased temperature gradient in the equatorial stratosphere), and thus stronger zonal winds, can divert wave activity equatorward which further strengthens the vortex (Borovko and Krupchatnikov (2009)).

If the vortex is sufficiently strong, its influence can extend down to the surface, causing a positive North Atlantic Oscillation/Arctic Oscillation. The North Atlantic Oscillation (NAO) is an index corresponding to the difference in MSLP between the Azores and Iceland (Rodwell et al. (1999)), and the Arctic Oscillation (AO) is defined as the first hemispheric empirical orthogonal function (EOF) of sea level pressure variability (Stenchikov et al., 2002). Essentially the NAO can be thought of as the AO over the Atlantic region, with the AO previously being termed as a global extension of the NAO (Christiansen (2008)). Positive values correspond to anomalously low pressure over the poles, and anomalously high pressure at the midlatitudes and hence a stronger East-West stormtrack (see figure 3.3 for a diagram of effects in positive

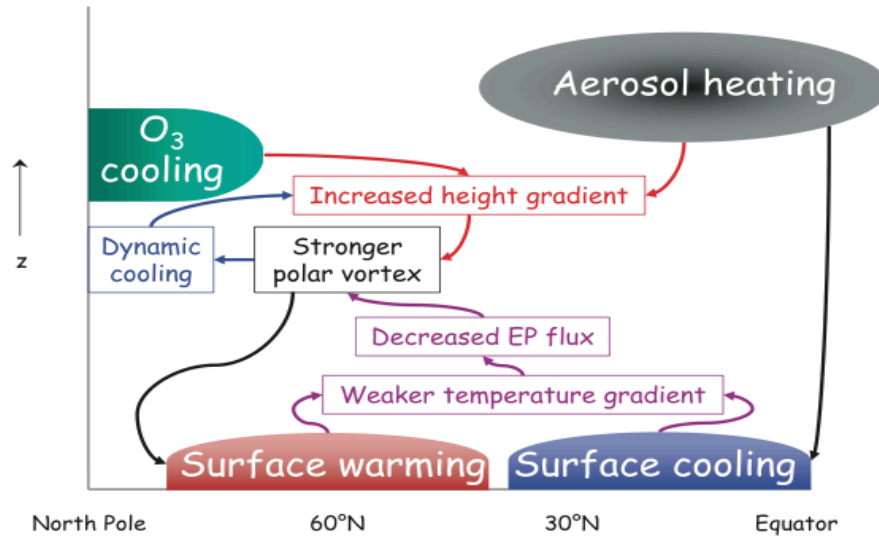


Figure 3.2: Schematic diagram illustrating the proposed volcanic mechanism from Stenchikov et al. (2002)

and negative AO phases). After large volcanic eruptions a positive phase of the AO has been observed for the following 1 to 2 winters (Stenchikov et al. 2002), and the stronger east-west winds cause advection of energy due to anomalous strong wind blowing warm oceanic air overland, and this causes an anomalously warm temperatures over major northern hemisphere landmasses. The effect of this changing circulation can be seen in the DJF temperature anomaly following Mount Pinatubo, shown in figure 3.4. The anomalous warming over NH land is typical for the two winters following a tropical volcanic eruption that injects into the stratosphere (Stenchikov et al. (2006)).

During a positive NAO the stormtracks also shift northwards, Northern Europe becomes warm and wet, whilst Southern Europe becomes dry (Walter and Graf (2005)). Christiansen (2008), analysed 13 volcano eruptions over the period 1883 to 1991 and found that the AO, the NAO and the Pacific North American Oscillation (PNA) are all positive in the first winter after eruptions. This is statistically significant for the NAO in particular, with both the numbers of events and their amplitudes being statistically significant. There has been some debate about which is physically more meaningful, for example Ambaum et al. (2001) and, interestingly, Christiansen (2008) concludes that from his results the NAO should be credited as the physical mode of

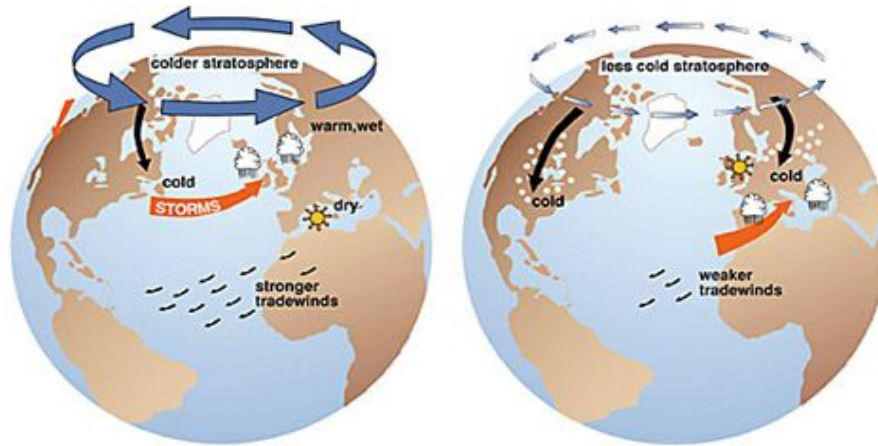


Figure 3.3: Some of the effects of a positive phase AO (left) and a negative phase (right)

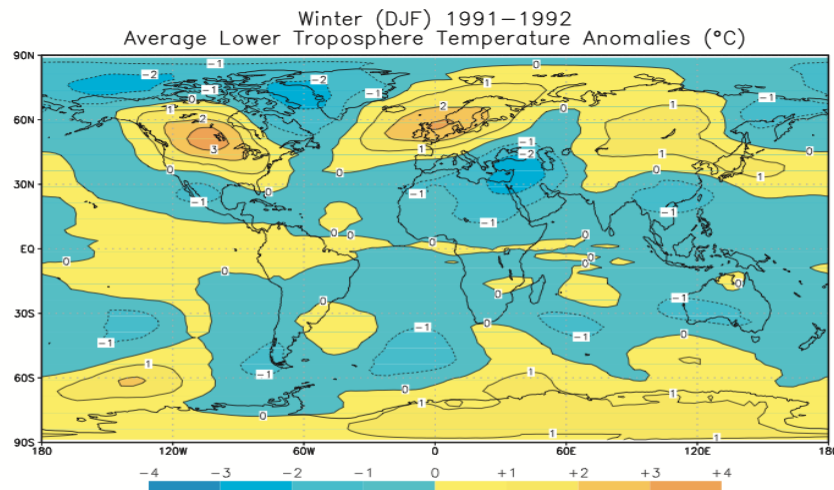


Plate 1. Winter (DJF) lower tropospheric temperature anomalies (with the non-volcanic period of 1984-1990 used to calculate the mean) for the 1991/92 Northern Hemisphere winters (DJF) following the 1991 Mt. Pinatubo eruption. This pattern is typical of that following all large tropical eruptions, with warming over North America, Europe, and Siberia, and cooling over Alaska, Greenland, the Middle East, and China. Data from Microwave Sounding Unit Channel 2R [Spencer *et al.*, 1990], updated courtesy of J. Christy and now called Channel 2LT. Anomalies greater than 1°C are shaded. (See the color version of this plate at the back of this volume.)

Figure 3.4: Post Pinatubo 1991-1992 DJF Temperature Anomalies from the 1984-1990 average showing anomalous surface warming over North America, Europe and Russia, from Robock (2003)

variability, with the interpretation that the NAO is excited following an eruption is more simple and economical than the alternative explanation that the AO and PNA patterns negatively interfere in the Pacific so as to cancel each other out to give the observed MSLP fields. However, it should be recalled that nonetheless both the NAO and the AO indexes are positive following volcanic eruptions. Large magnitude values of the AO are associated with significant changes in the likelihoods of extreme

weather events, such as cold air outbreaks, snow and high winds across Europe, Asia and North America, as well as modulating the position of surface cyclones over the Atlantic and Europe (Baldwin and Dunkerton (2001)).

As mentioned, the Pinatubo eruption caused serious effects on the hydrological cycle, namely a large decrease in precipitation and a period of record decrease in runoff and river discharge into the ocean (Trenberth and Dai, 2007). They note that this is of concern for sulphate aerosol geoengineering studies - in contrast with the view of Wigley (2006) who suggested that the Mount Pinatubo did not severely disrupt the climate system. Figure 3.5 shows changes to precipitation, runoff and the Palmer Drought Severity Index (PDSI) following Mount Pinatubo from Trenberth and Dai (2007). The PDSI is a diagnostic developed by Palmer (1965). A measure of drought in the region, it incorporates not only drought in a region but other measures such as evapotranspiration into a single diagnostic, and can be seen as a more complete assessment of the effects on hydrology than precipitation, and is an important diagnostic for assessing water availability in a region (see Palmer (1965) for extensive documentation). Precipitation effects are not purely radiatively driven, but indeed the effects of the dynamical response to a volcanic eruption on precipitation in the Asian monsoon region can often overwhelm the radiative effects on precipitation (Anchukaitis (2010)). Baldwin and Dunkerton (1999) note that a positive AO causes storm tracks to move north, and we later demonstrate that the observed strengthened NH polar vortex and positive NAO pattern is consistent with a shift in the storm tracks and drought in the European region. Despite the importance of the hydrological cycle, both in the functioning of the climate system and for society, there have been far fewer investigations on the hydrological cycle than on radiative and dynamical studies on the effects of volcanoes. Indeed, the author is aware of only three studies on rainfall that include volcanoes (Trenberth and Dai (2007), Gu et al. (2007), Anchukaitis (2010)), which focus on Pinatubo alone, the zonal averaged response in latitude bands for El Chichon and Pinatubo (but for purposes of removing the volcanic signal to assess variability), and the Asian Monsoon response as assessed from proxy reconstructions, respectively. None of these assess the composite observations and model simulations over the globe. Compare this with

studies on radiation and dynamics, for example, Robock and Mao (1992), Graf et al. (1993), Stenchikov et al. (1998), Timmreck et al. (1999), Stenchikov et al. (2002), Stenchikov et al. (2004), Stenchikov et al. (2006), Robock et al. (2007), Graf et al. (2007), Ottera (2008), Robock et al. (2009), Kravitz et al. (2011), and so on.

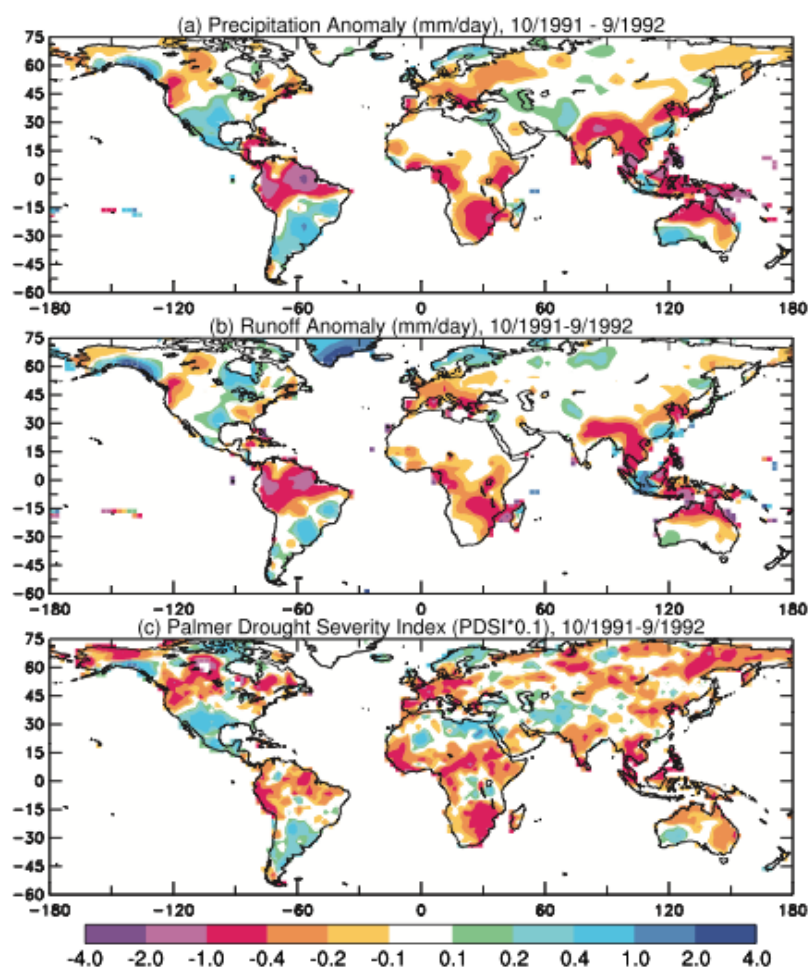


Figure 3. (a) Observed precipitation anomalies (relative to 1950–2004 mean) in mm/day during October 1991–September 1992 over land. Warm colors indicate below normal precipitation. (b) As for Figure 3a but for the simulated runoff [Qian et al., 2006] using a comprehensive land surface model forced with observed precipitation and other atmospheric forcing in mm/day. (c) Palmer Drought Severity Index (PDSI, multiplied by 0.1) for October 1991–September 1992 [Dai et al., 2004]. Warm colors indicate drying. Values less than -2 (0.2 on scale) indicate moderate drought, and those less than -3 indicate severe drought.

Figure 3.5: (a) Precipitation and (b) Runoff Anomalies, and (c) Palmer Drought Severity Index following Pinatubo, from Trenberth and Dai (2007)

3.1.1 Ocean Response

Following the reduced surface flux of radiation into the Oceans caused by a volcanic eruption, ocean heat content and sea level can reduce (Gleckler et al. (2006), Stenchikov et al. (2007)). The cooling of the surface subducts downwards into the ocean (Gleckler, et al. (2006)) where the signal persists for decades. The relaxation process for the SST's to return to close their unperturbed climate state from model simulations has been estimated at about ten years from model simulations (Stenchikov et al., (2009)). However the entire relaxation process for the whole ocean might take more than a century (Stenchikov et al. (2009)).

Decrease in precipitation following volcanic eruptions causes increased ocean salinity whilst the reduced temperatures increase the density of the northern hemisphere high latitude upper ocean, causing vertical instability and encouraging ocean convection. Moreover, increased zonal winds in the NH following a volcanic eruption causes a strengthening of ocean stirring in high latitudes. Therefore, volcanoes, can increase the strength of the Atlantic Meridional Circulation (AMOC) (Stenchikov et al. (2009)). The model simulations performed by Stenchikov et al. (2009) found a maximum increase in the AMOC of 2.7 Sverdrup (Sv) and 1.8 Sv for the 1816 Tambora and 1991 Pinatubo eruptions respectively. The decadal time scales of this circulation mean that the maximum occurs at 5-15 years post-eruption. Their simulations also show increases in sea-ice extent and mass following a volcanic eruption - consistent with geoengineering studies demonstrating that sulphate aerosol geoengineering could reduce sea ice loss. A possible cause for concern for modelling studies and also controllability of sea ice under a sulphate geoengineering scenario, however, is that Stenchikov et al. (2009) note that the radiative forcing effects on sea ice extent are less than linear as the sea ice is also affected by ocean circulation changes that are nonlinear.

Negative surface temperature anomalies in the Middle East are a distinctive feature of the positive phase of the AO caused by a volcanic eruption (e.g. Robock (2000), Stenchikov et al. (2006), Fischer et al. (2007)). Correspondingly, the resulting dynamical changes following a volcano can be important for ocean circulation and ecosystems. Robock (2003) suggests that such a large local cooling followed

the Pinatubo eruption that the Red Sea underwent a total overturning, killing all the coral at the seabed. This is also an important feedback to capture in a geo-engineering modelling study. However, the strong sporadic forcing from a volcano intensifies vertical mixing processes, notably turbulent diffusion, seasonal convection and overturning, whilst a constant forcing of the same average intensity, such as that in a geoengineered world, may produce a different vertical ocean thermal structure (Stenchikov et al. (2009)).

3.1.2 Interactions with ENSO and the QBO

Of the past four major eruptions - Agung (1963), Fuego (1974), El Chichon (1982) and Pinatubo (1991) - two of them (El Chichon and Pinatubo) have erupted during the El Nino phase of the El Nino Southern Oscillation (ENSO, Robock (2000)). ENSO is a major mode of atmospheric variability, characterised by sea surface temperature changes off the west of coast of South America in the tropics. It is often hard to separate the signals between volcanoes and ENSO particularly due to low numbers of well observed volcanic eruptions, and the contribution to the resultant effects on climate and the NAO phase is not completely clear (Graf et al. (2007)). The polar vortex has been suspected to be influenced by ENSO (e.g. Thomas et al. (2009)), by an increased flux of planetary waves propagating up through the troposphere and into the stratosphere during El Nino (which then propagate towards the vortex and weaken it) (Graf et al. (2011)). Graf and Zanchettin (2011) also identify a tropospheric pathway, in identifying a "subtropical bridge" where planetary wave activity can propagate through the troposphere and affect the NAO pattern. Therefore, it is possible that ENSO can obscure the true volcanic signal not only in the tropics but also over the Northern Hemispheric continents. Christiansen analysed 13 volcanic eruptions since 1883 to present day, and assess the role that ENSO plays in the NAO signal in observations. He concludes that the NAO and AO signals are both positive and statistically significant for the first winter after an eruption. He finds no evidence that the ENSO phase influences the NAO following a volcanic eruption - although adds that due the low numbers of ensembles, this result should be treated with caution.

The Quasi-Biennial Oscillation (QBO), has also been suggested to have an influence on the effect of volcanic eruptions on climate (e.g. Stenchikov et al. (2004), Thomas et al. (2009)). The QBO is the major mode of tropical stratospheric variability. It is a cycle of the equatorial zonal wind in the tropical latitudes in the stratosphere, where the winds switch from easterlies to westerlies and back to easterlies, and so on, in a quasi-periodic fashion on average every 28 to 29 months. The easterly, or westerly, winds develop in the upper stratosphere, around 3hPa, and then propagate downwards (Baldwin et al. (2001)). Evidence that westerly QBO winds cause a stronger polar vortex, stem from research originally conducted by Holton and Tan (1980, 1982) and McIntyre (1982). The hypothesis states that westerly winds in the equatorial regions allow the propagation of planetary waves from the midlatitude and polar regions, through the lower equatorial stratosphere, whilst easterly equatorial waves block the propagation of these planetary waves and guide them polewards so that when they eventually break they are more likely to disturb the vortex. Therefore it is believed the vortex, and hence the NAO, can be strengthened or weakened, depending on the QBO state.

Stenchikov et al. (2004) detail that following the Mount Pinatubo eruption the vortex in both winters was strengthened relative to climatology. Despite a significant decline in the radiative aerosol forcing in second winter the vortex was observed to be stronger in the second winter than in the first winter. They therefore propose that the QBO played a role in the vortex being stronger in the second winter than in the first - noting that the QBO was in an easterly phase in the first winter and westerly phase in the second winter. They perform model simulations of the Mount Pinatubo nudging the simulated equatorial winds to the observed winds, and note that this achieves a more strengthened vortex in the second winter. They conclude that modelling the correct phase of the QBO is crucial for simulating the temperature change in the lower stratosphere. Moreover, they note that the volcanic aerosol and QBO effects are unlikely to be a simple linear superposition of the two effects, due to a threshold dependence of the refraction of planetary waves on the strength of the polar night jet. Other studies have also suggested that the QBO could have a significant modulation on the volcanic effect on climate (e.g. Thomas et al. (2009)). However,

whilst in their study Thomas et al. (2009) investigate the effect of the phases of the QBO on the stratosphere in model simulations and find, similarly, that an easterly QBO phase leads to a weaker vortex during volcanic winters.

An additional source of complexity in identifying the volcanic signal on climate, changes in the solar cycle have been seen to cause changes in stratospheric temperatures and winds and there is a complex interaction between the 11-year solar cycle and the QBO which is not fully understood and has yet to be successfully simulated by climate models (Gray et al. (2010)). There are only 4 well observed large eruptions (Agung, 1963, Fuego, 1974, El Chichon, 1982, and Pinatubo, 1991) and solar maxima have occurred close to the times of Fuego, El Chichon and Pinatubo (Solomon et al. 1996). Indeed, it has been noted that more work remains to assess the dynamical interactions between all these modes of variability and the atmosphere following a volcano eruption (e.g. Graf et al. (2007)).

3.1.3 Simulations of Climate following Volcanic Eruptions

Climate models have traditionally not simulated the observed response to stratospheric aerosol loading caused by volcanic eruptions sufficiently. Stenchikov et al. (2006) analysed seven models used for the fourth assessment report that were uploaded to the Coupled Model Intercomparison Project 3 (CMIP3). These were all the models that specifically included representation of volcanic eruptions by including a layer of aerosol, instead of either not representing them, or representing them simply by a reduction in the solar constant. They found that the lower equatorial stratospheric temperature increase, caused by radiative heating from the aerosol, is represented in all the models sampled. However, the models showed less of an agreement with the observed post eruption northern hemisphere winter northern lower polar stratospheric cooling. Further, the 50hPa geopotential height anomalies in the models generally show almost no anomaly relative to climatology whereas the observations show a very large negative anomaly of about 200m, indicative of an anomalously strong stratospheric polar vortex. Furthermore, the climate model simulated responses of the AO are significantly weaker than in observations. Correspondingly

the surface temperature anomalies related to observed dynamical changes are not sufficient in strength and spatial pattern in the CMIP3 models. Other simulations and assessments of why models fail to get the response have been done, such as those of Stenchikov et al. (2002), Stenchikov et al. (2004) that also show too weak a response when compared with observations.

Many proposals have been made as to why the vortex, AO, and surface response has not been captured in models, however it is presently not clear why dynamical effects are not captured (Marshall et al. (2009)). Stenchikov et al. (2004) suggested the lack of a QBO could have an important effect on atmospheric processes following a volcanic eruption. Marshall et al. (2009) proposed that the climatology of the models may be inaccurate. Notably they suggest propagation of planetary waves from the troposphere into the stratosphere may be too large, such that it breaks and destabilises the vortex. Stenchikov et al. (2006) suggested that all but one of the models they analysed had winds that were too strong at 50hPa averaged over 55 – 65° N, when compared to observations. Therefore, they state that perhaps the winds in the models are too strong climatologically, which means there is a bias towards a positive AO, so therefore when a volcanic eruptions occurs, there is little anomalous effect on the AO. Ottera (2008) suggested that models may simply fail to get a sufficiently strong positive AO to external forcings in general (also Graf (*personal communication*)), noting that many models have failed to reproduce the observed trend in the AO during the latter part of the twentieth century (see Shindell et al. (2001) for more details), however this fails to explain why the models do not achieve a sufficiently strengthened polar vortex, and it is not clear whether the observed AO trend is real (e.g. Fyfe et al. (2013)). Stenchikov et al. (2006), Ottera (2008) and Marshall et al. (2009) suggested stratospheric resolution may be important for capturing the relevant processes following a volcanic eruption. Dall’Amico et al. (2010) note that stratospheric processes in model simulations as recent as those used by the Intergovernmental Panel on Climate Change Fourth Assessment Report have been poorly represented. Whilst the stratopause height is typically around 1hPa (Andrews et al. 1987) around half the Atmosphere and Ocean General Circulation Models (AOGCMs) used for the AR4 have a model top level beneath 2hPa, and furthermore

show significant cold bias around their 10hPa levels suggesting compromised simulations in these regions due either to a low model top or insufficient stratospheric levels (Cordero and Forster (2006)). Specifically with regards to models used in previous volcanic investigations, of the seven models tested by Stenchikov et al. (2006) two of the models (GISS-EH, GISS-ER) have lid heights above the 1Pa level (at both 0.1hPa, or roughly 70km, each), whilst all the other models have model lid heights below the stratopause level - GFDL CM 2.0 (3hPa), GFDL CM2.1 (3hPa), NCAR CCSM3 (2.2hPa), NCAR PCM1 (2.9hPa), MIROC-medres (10hPa). Also note that although the top lid of these latter models may appear to include most of the stratosphere, the vertical resolution of the model is usually severely degraded at these upper levels and there is strong damping applied to any wave disturbances. Other suggestions as to why models have traditionally failed to simulate the observed response following volcanic eruptions include realistic changes in ozone which cause additional cooling of the stratospheric polar vortex (e.g. Ottera 2008), however, as noted by Marshall et al. (2009) the response to the past major eruptions (before major ozone loss and larger amounts of ozone destroying chlorine in the atmosphere) is similar to that of El Chichon and Pinatubo combined. Thus it is less likely for ozone inclusion to be a major factor in the simulation of a volcanic eruption. Finally, another proposal has been that of the realism of the aerosol implemented in the models is not sufficient (Ottera (2008), Marshall et al. (2009), Toohey et al. (*in prep/personal communication*)). Marshall et al. (2009) also assessed the possibility that the strengthened vortex and positive NAO following volcanic eruptions was due to internal variability, but they conclude it is ‘extremely unlikely’ to be an artifact of internal variability, and so it is extremely likely that models are failing to capture a robust high-latitude climate response to volcanically injected sulphate aerosol.

It is clear, therefore, that not only are models are failing to reproduce the observed response to stratospheric sulphate aerosol injected by volcanic eruptions - of concern for the accuracy of sulphate aerosol geoengineering modelling studies - and there is no single clear reason as to why this is the case, but also the precise response of the atmosphere to sulphate aerosol loading is unclear.

3.2 Observations and Model Assessment

3.2.1 Observed response to Volcanic Eruptions in the ERA40 dataset

Previous investigations have focused mainly on the NCEP/NCAR dataset (e.g. Stenchikov et al. (2006), Graf et al. (2007), Ottera (2008)), with only Thomas et al. (2009) using the ERA40 dataset for post Pinatubo analysis. Here we investigate volcanic eruptions as in the ERA40 dataset. We also make comparisons with composites in the ERA40 dataset and the composites with NCEP/NCAR as calculated in previous papers to assess ERA40's performance over the past four eruptions. For the individual eruptions we focus only on 1.5 metre temperature and MSLP anomalies (figures 3.6 and 3.7 respectively) which are the most important for the impacts of volcanic eruptions. For the composites we also include the anomalies of 50hPa geopotential height, indicative of stratospheric polar vortex strength.

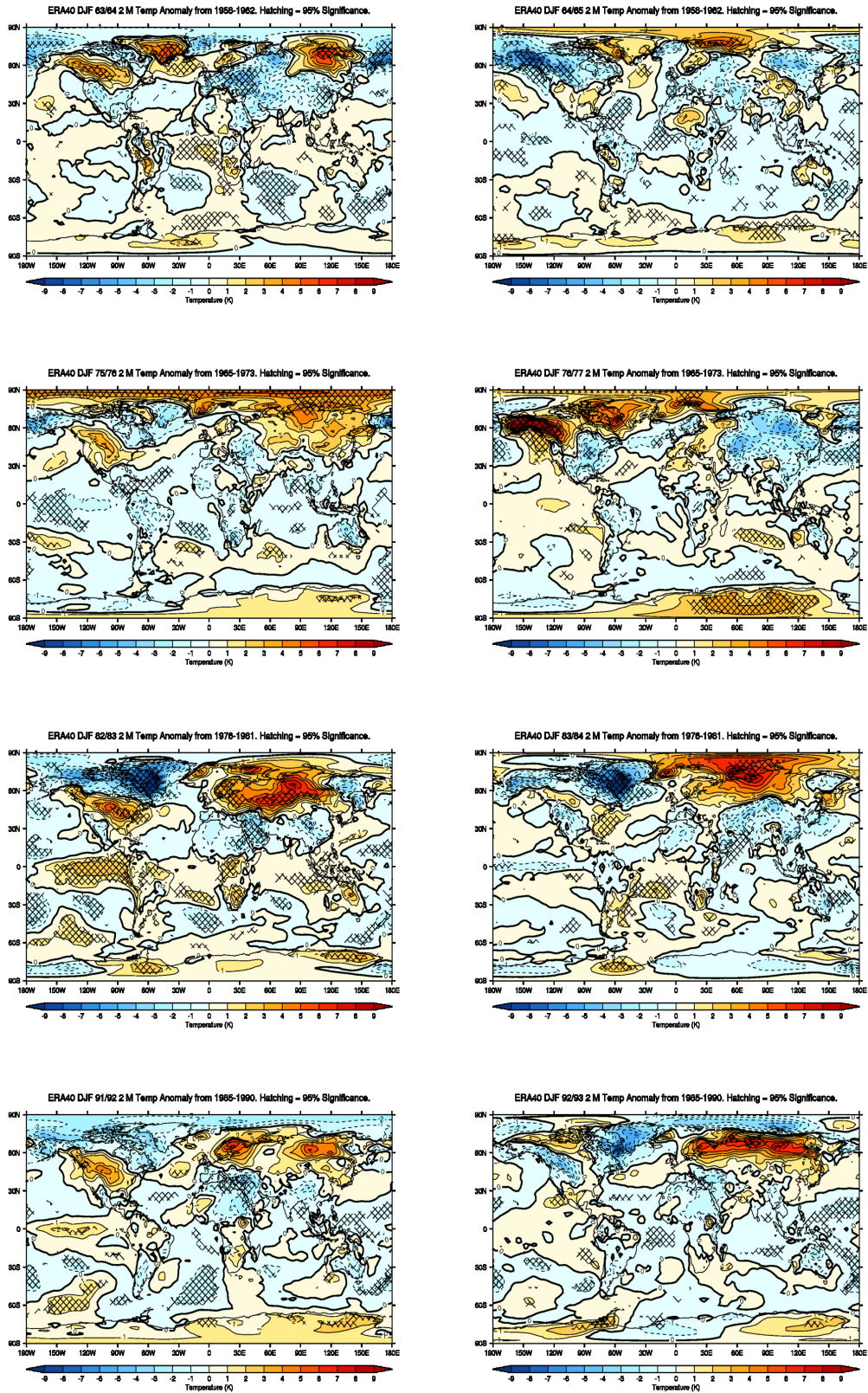


Figure 3.6: ERA40 2 M Temperature Anomalies for Agung (top row), Fuego (second row), El Chichon (third row) and Pinatubo (fourth row). Left column is the first winter following the eruption, right column is the second winter. Hatching displays areas at or over 95 per cent significance.

Table 3.1 lists the nine major low latitude volcanic eruptions over 1883-present day, of which ERA40 covers the last four, as well as the anomaly period, and the latitudes of eruption, for which anomalies are then created by the difference between the volcanic winter and the appropriate reference period listed in the table. Information for this is taken from Stenchikov et al. (2006). We see that figure 3.6 reveals the NH DJF Eurasian warming in the first Fuego winter, and all of the winters of the considerably larger El Chichon and Pinatubo volcanic eruptions. Large North American warming is also evident in many of the winters. It should be noted that there is reasonable variation in the spatial patterns and that noise can obscure single winter anomalies. MSLP fields (figure 3.7) also reveal positive NAOs in all winters with warming, and a positive NAO is absent in the winters where there is not surface warming. Values for temperature, MSLP and geopotential height can be seen to have extremely close agreement to that of NCEP/NCAR values as shown in Stenchikov et al. (2002), Ottera (2008) and Thomas et al. (2009).

Table 3.1: Major low latitude eruptions over 1883 to present day

Volcano	Eruption Date	Latitude	Appropriate Winters to Analyse	Reference Period
Krakatau	Aug 27, 1883	6.10°S	1883-1884 1884-1885	1860-1882
Tarawera	Jun 10, 1886	38.23°S	1886-1887 1887-1888	1860-1882
Bandai	Jul 15, 1888	37.60°N	1888-1889 1889-1890	1860-1882
Santa Maria	Oct 24, 1902	14.76°N	1903-1904 1904-1905	1890-1901
Quizapu	Apr 10, 1932	35.65°	1932-1933 1933-1934	1915-1931
Agung	Mar 17, 1963	8.34°S	1963-1964 1964-1965	1934-1955
Fuego	Oct 10, 1974	14.47°N	1975-1976 1976-1977	1965-1973
El Chichon	Apr 4, 1982	17.36°N	1982-1983 1983-1984	1976-1981
Pinatubo	Jun 15, 1991	15.13°N	1991-1992 1992-1993	1985-1990

Composite values of the 1.5 M Temp, MSLP and 50hPa Geopotential Height following the four eruptions are shown in figure 3.3. Composite values in ERA40 reveal a large winter warming of up to 4K over Eurasia, and cooling over the Middle Eastern region. Also evident is a warming over the west coast of North America. There is a warming over the pacific tropical region which could be due to the large

number of El Ninos that took place both during and after the eruptions. MSLP fields reveal a strong positive NAO significant at the 95 per cent level, whilst anomalies on the 50hPa geopotential height surface reveal large negative polar anomalies around -200m, indicative of the stronger polar vortex that is suggested in the theory.

Despite this, observations are still too few for good statistics on interactions with the NAO, QBO and ENSO. We therefore take advantage of the new NOAA Twentieth Century Reanalysis Version 2 Observation Dataset (Compo et al. 2011) (NOAA from now on). This is a 3D global reanalysis dataset that extends from January 1871 to December 2008 but the only observed surface variables are assimilated. It assimilates only observed surface variables and then creates 3D global analysis that is the most likely state of the atmosphere at that time. As a test of viability, figures 3.6 and 3.7 display temperature and MSLP anomalies following the four most recent volcanoes calculated in exactly the same way as figures 3.1 and 3.2 were for ERA40. Thus one can see that the figures display good agreement between ERA40 and NOAA in the surface variables' anomalies and statistical significance during the period in which there is overlap between the two datasets. Extending the analysis back to 1883, we focus predominantly on surface variables because without satellites a great deal of stratospheric information must be provided by a model and cannot be trusted as a suitable assessor for a model's performance. Values of 2 M Temperature and MSLP are plotted in figure 3.11 for NOAA for the 9 most recent eruptions allowing us to assess the robustness of the signal across more volcanic eruptions. Also plotted in figure 3.11 are the 50hPa geopotential height anomalies, although these are provided for 'completion'.

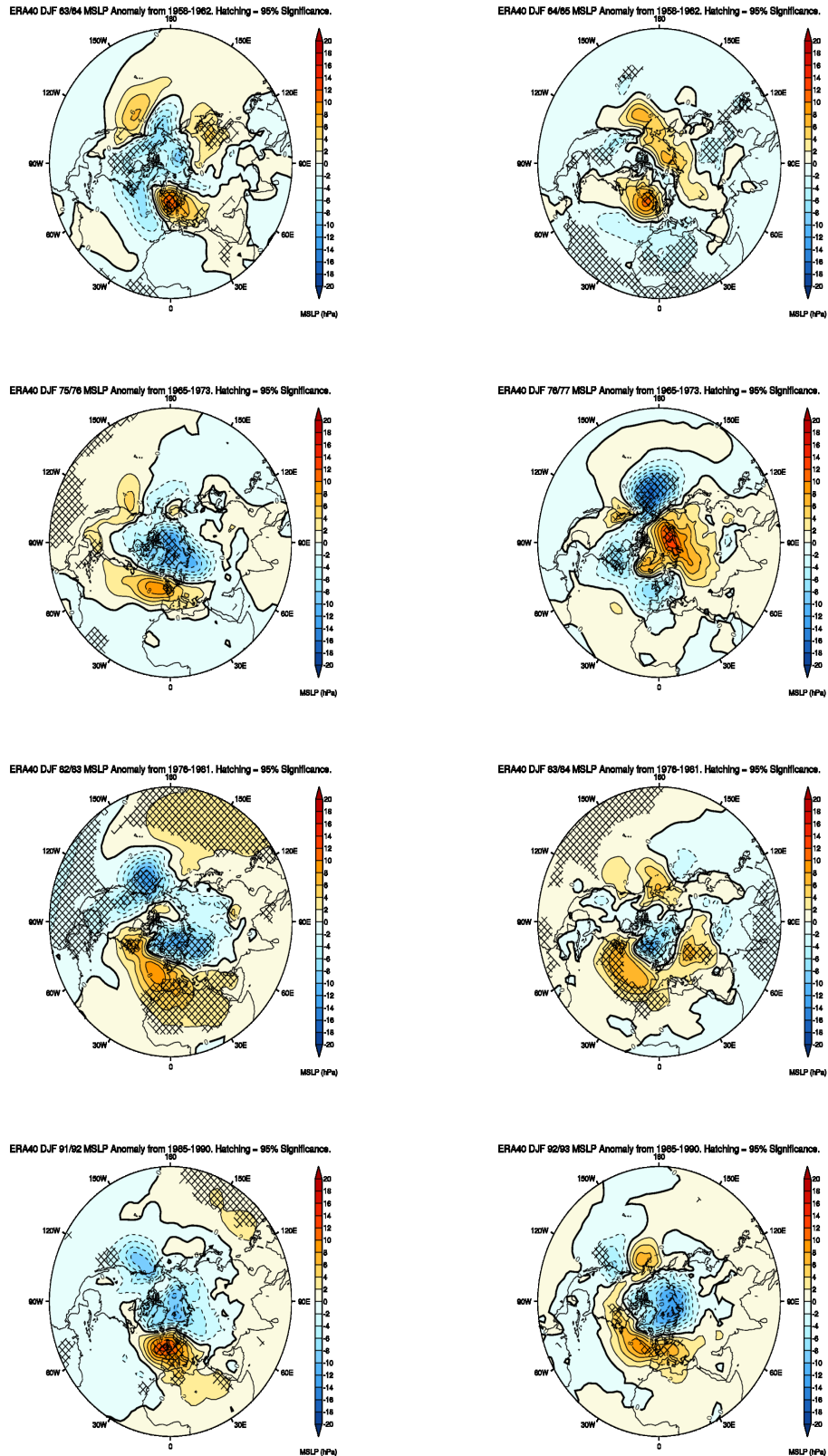


Figure 3.7: ERA40 MSLP Anomalies for Agung (top row), Fuego (second row), El Chichon (third row) and Pinatubo (fourth row). Left column is the first winter following the eruption, right column is the second winter. Hatching displays areas at or over 95 per cent significance using a two-tailed t-test.

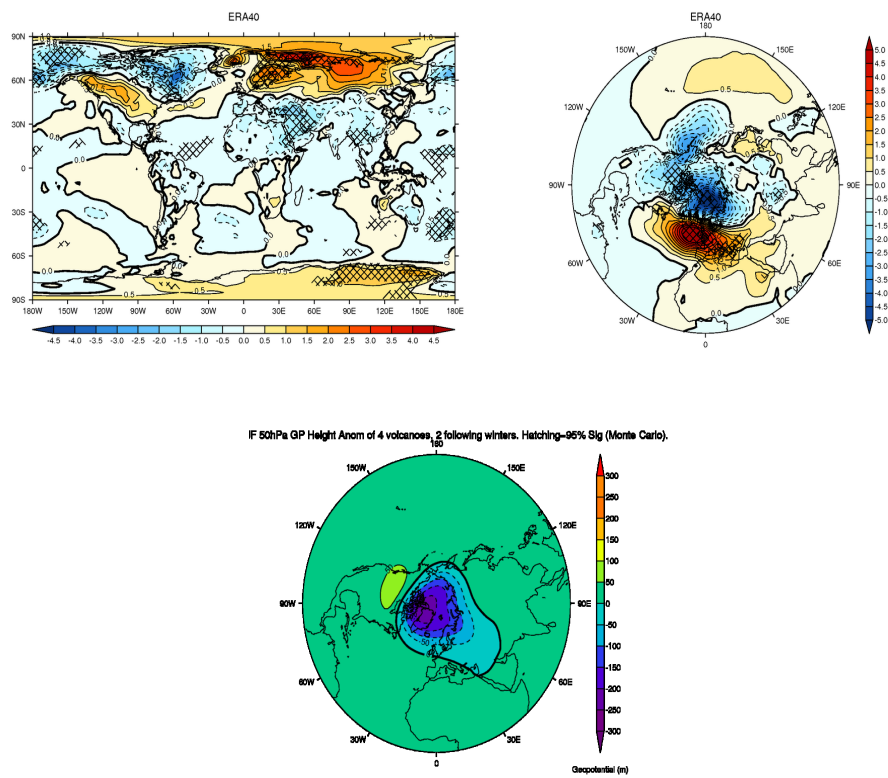


Figure 3.8: ERA40 composite anomalies of 2 M Temperature (top left), MSLP (top right) and 50hPa Geopotential Height (bottom) for the two following winters for all the past four major eruptions (8 winters total). Hatching displays areas at or over 95 per cent significance using a two tailed t-test.

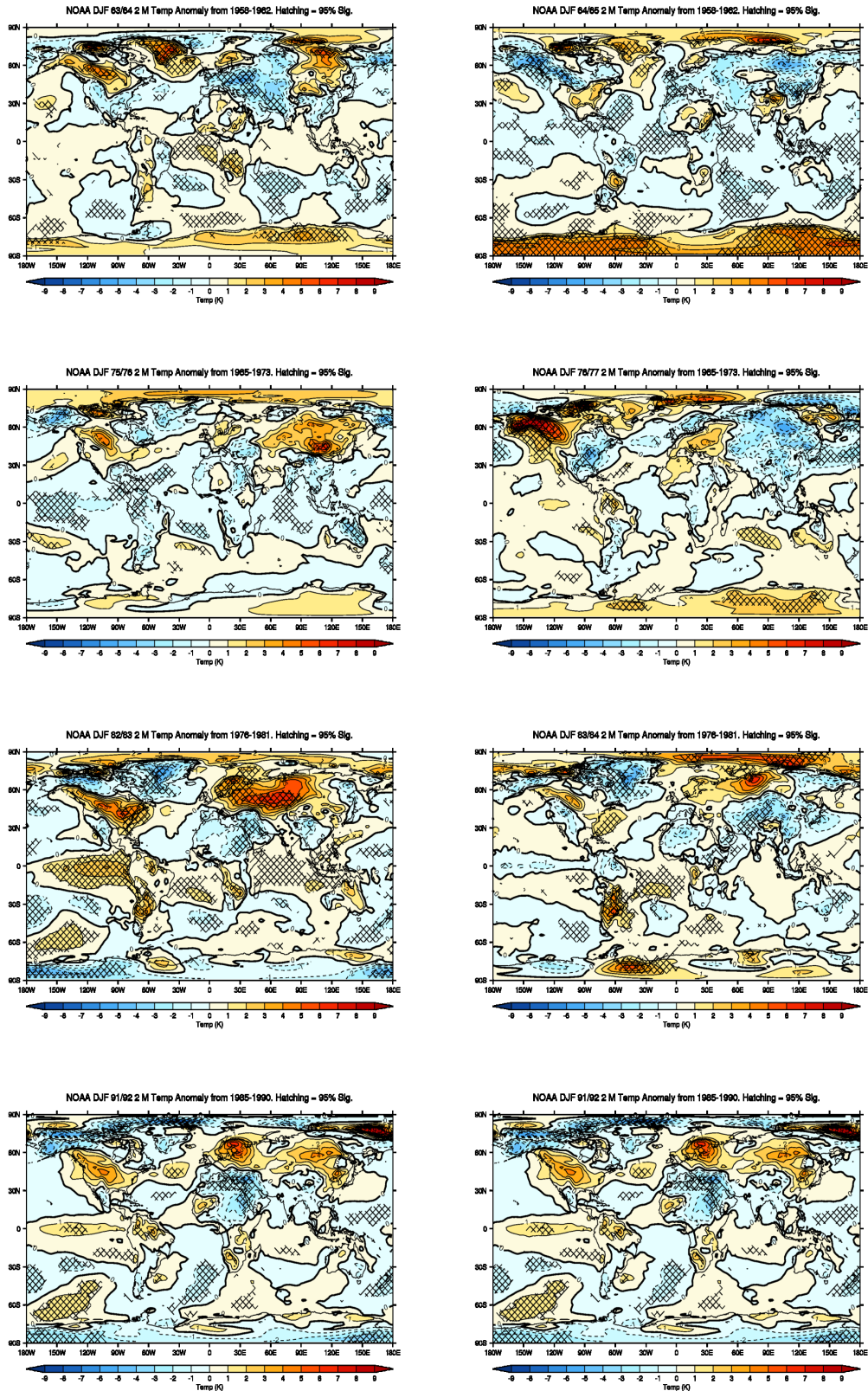


Figure 3.9: NOAA 2 M Temperature Anomalies for Agung (top row), Fuego (second row), El Chichon (third row) and Pinatubo (fourth row). Left column is the first winter following the eruption, right column is the second winter. Hatching displays areas at or over 95 per cent significance.

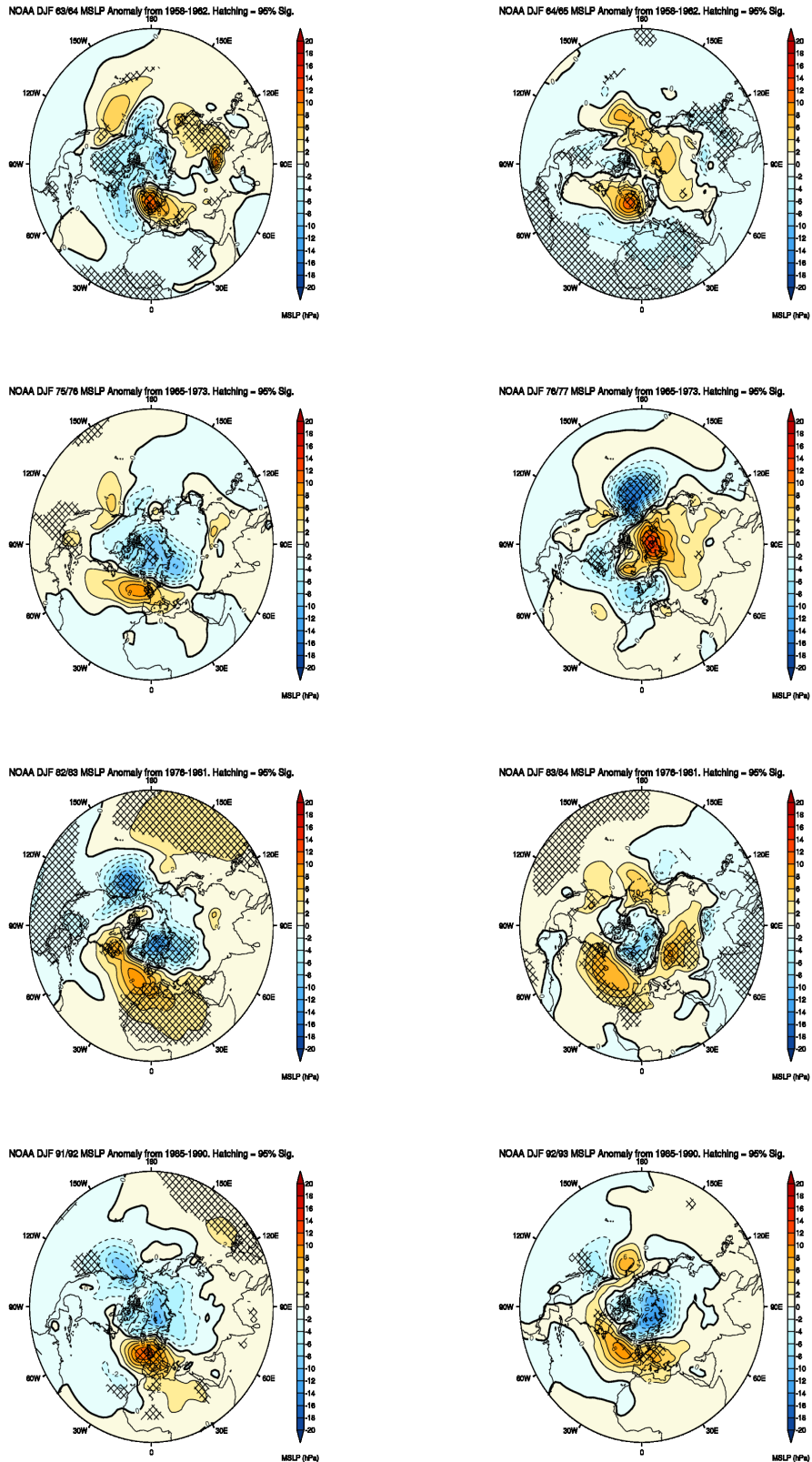


Figure 3.10: NOAA MSLP Anomalies for Agung (top row), Fuego (second row), El Chichon (third row) and Pinatubo (fourth row). Left column is the first winter following the eruption, right column is the second winter. Hatching displays areas at or over 95 per cent significance.

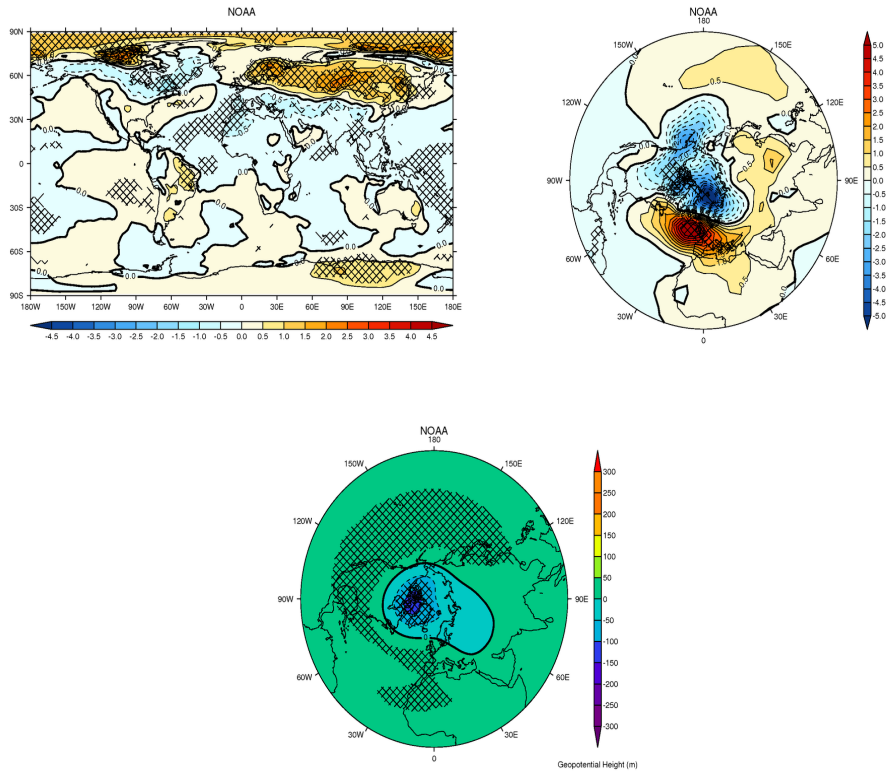


Figure 3.11: NOAA composite anomalies of 2 M Temperature (top row), MSLP (second row) and 50hPa Geopotential Height (bottom row) for the two following winters for the past four most recent major eruptions (left column) and past nine most recent major eruptions (right column). Hatching displays areas at or over 95 per cent significance using a two tailed t-test)

It can be seen that following 9 volcanic eruptions near surface temperature anomalies reveal a statistically significant Eurasian warming pattern, and positive and statistically significant NAO signal, and reduce geopotential heights at the poles are consistent with the positive NAO following volcanic eruptions. The composite anomalies in NOAA are slightly smaller than in ERA40 data, yet there is good agreement between the two datasets. The NOAA dataset allows us to perform a more statistically robust analysis on some aspects of dynamical interactions of the climate.

3.2.2 Impact of the QBO on the NAO following volcanic eruptions

The issue of dynamical interactions between the QBO and volcanic aerosol effects and understanding these interactions is also of great importance when considering the dynamical response of the atmosphere to volcanic eruptions. The QBO, an oscillation of winds from Easterly to Westerly with an average period of 28 to 29 months, has a profound influence on stratospheric dynamics and has been postulated as being of very large importance with regards to the interpretation of the volcanic response (e.g. Stenchikov (2004), Thomas et al. (2009)). However, previously no investigation has studied the effects that the QBO has on surface variables following a volcanic eruption from observations. Here, we exploit the NOAA dataset to assess the impact of the QBO on the resulting climate following a volcanic eruption. The NOAA dataset does not have a QBO pattern due to the way the reanalysis product is calculated - a zonal wind for a ten year sample period is shown in Figure 3.12. Therefore, a second dataset is employed. Brönnimann et al. (2007) produced an observational dataset of the QBO back to the year 1900 using historical pilot balloon data. This dataset is used to provide information on the QBO phase for the major tropical volcanic eruptions during the period covered by the NOAA dataset and the dataset produced by Brönnimann et al. (2007). Defining a West QBO or East QBO winter as one with zonally averaged equatorial winds at 30hPa of greater than or less 5ms^{-1} during December, and splitting the Brönnimann et al. (2007) dataset into East and West QBO cases gives 5 and 4 volcanic winter composites, respectively. For 3 post-volcanic winters these winds are neither greater nor less than 5ms^{-1} . Whilst this represents a

modest number of samples, it is equal to the number of individual winters composites deemed sufficient and used by Ottera (2008) to assess the performance of the AGCM ARPEGE/IFS model in its ability to simulate volcanic eruptions. It also permits a greater number of samples than provided in previous datasets such as ERA40 or NCEP/NCAR (see Kalnay et al (1996) and Kistler et al. (2001) for details), and represents the largest possible number of observational samples currently available for the QBO during volcanic winters.

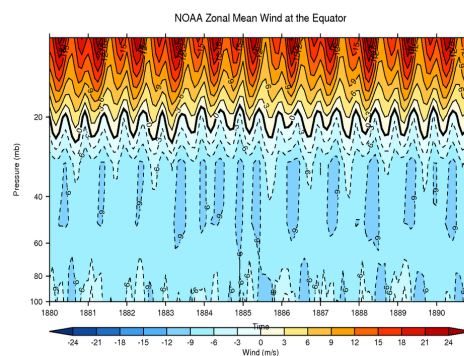


Figure 3.12: NOAA Zonal Mean Zonal Wind at the Equator for the ten year period of 1880-1890.

Combining the MSLP and 2 M Temperature of the NOAA dataset with that of Brönnimann et al. (2007) for QBO phase information one can construct anomalies of MSLP and 2 M Temperature according to the phase of the QBO. Figure 3.13 displays anomalies of 2 metre DJF temperature and MSLP of Easterly and Westerly phase QBO's using all years over the period of 1900-2005 from detrended climatology. Hatching shows areas that are statistically significant at the 99% level using a Monte Carlo significance test.

The composite anomalies of the East and West QBO winters shown in figure 3.13 reveal that there is little influence of the QBO on 2 M temperature. The East QBO phase shows slightly cooler temperatures over Africa and generally over Eurasia, which is the opposite in the West QBO phase, but the anomalies are extremely small, almost nowhere are values significant, with the exception of a warming of about 0.5K in Eastern North America and a small region of statistically significant cooling over

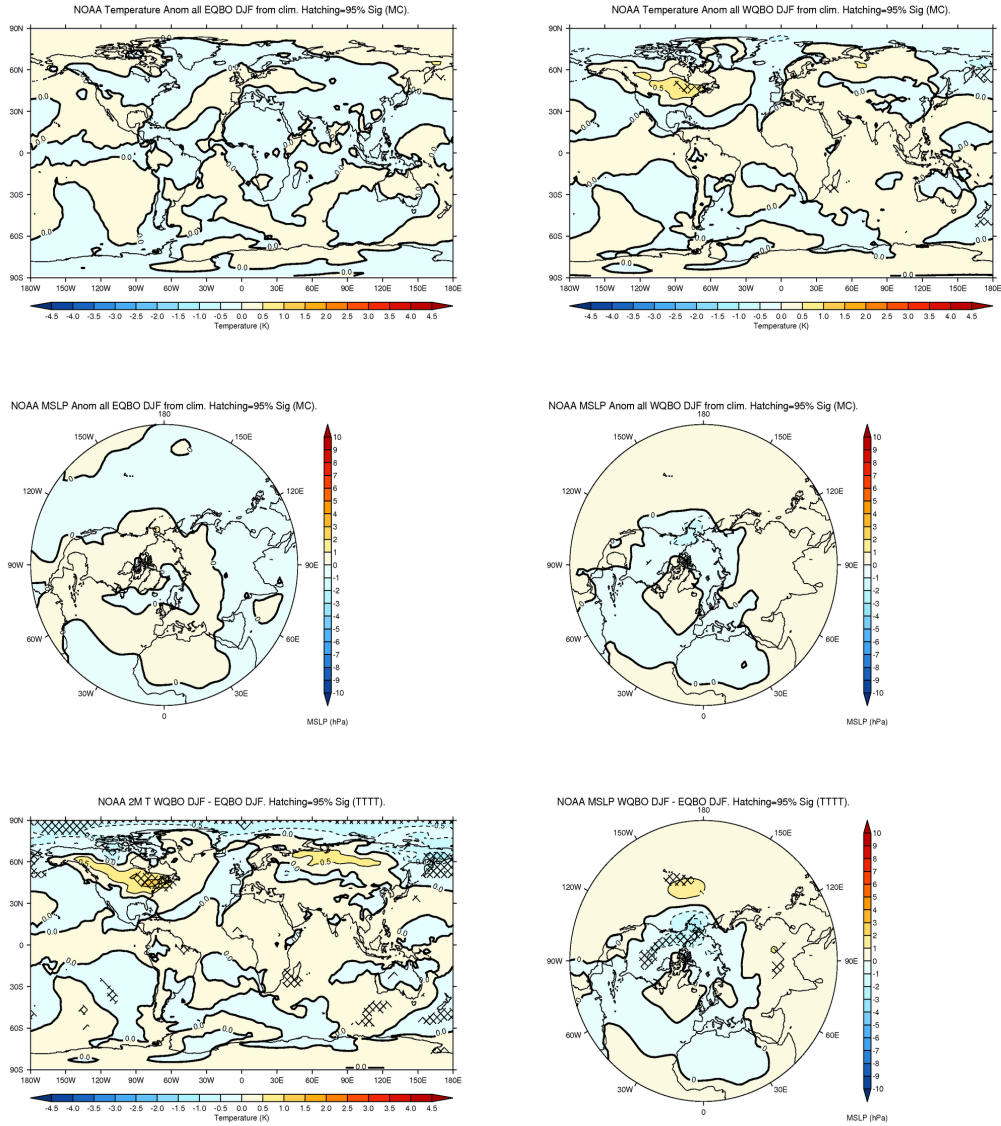


Figure 3.13: NOAA Composite Anomalies for East and West QBO Phase. First row displays 2 M temperature anomalies of all East QBO (left) and West QBO (right) winters from climatology. Third row displays MSLP anomalies of all East QBO (left) and West QBO (right) winters from climatology. Third row displays the difference plots of the West QBO field subtracted from the East QBO field for temperature (left) and MSLP (right). Hatching displays areas at or over 99 per cent significance using a Monte Carlo significance test.

the West Polar Pacific region and near far East Russia. Additionally, the MSLP fields reveal very little influence of the QBO at the surface. Differences between the two composites (i.e. the West QBO composite 2 metre Temperature and MSLP fields

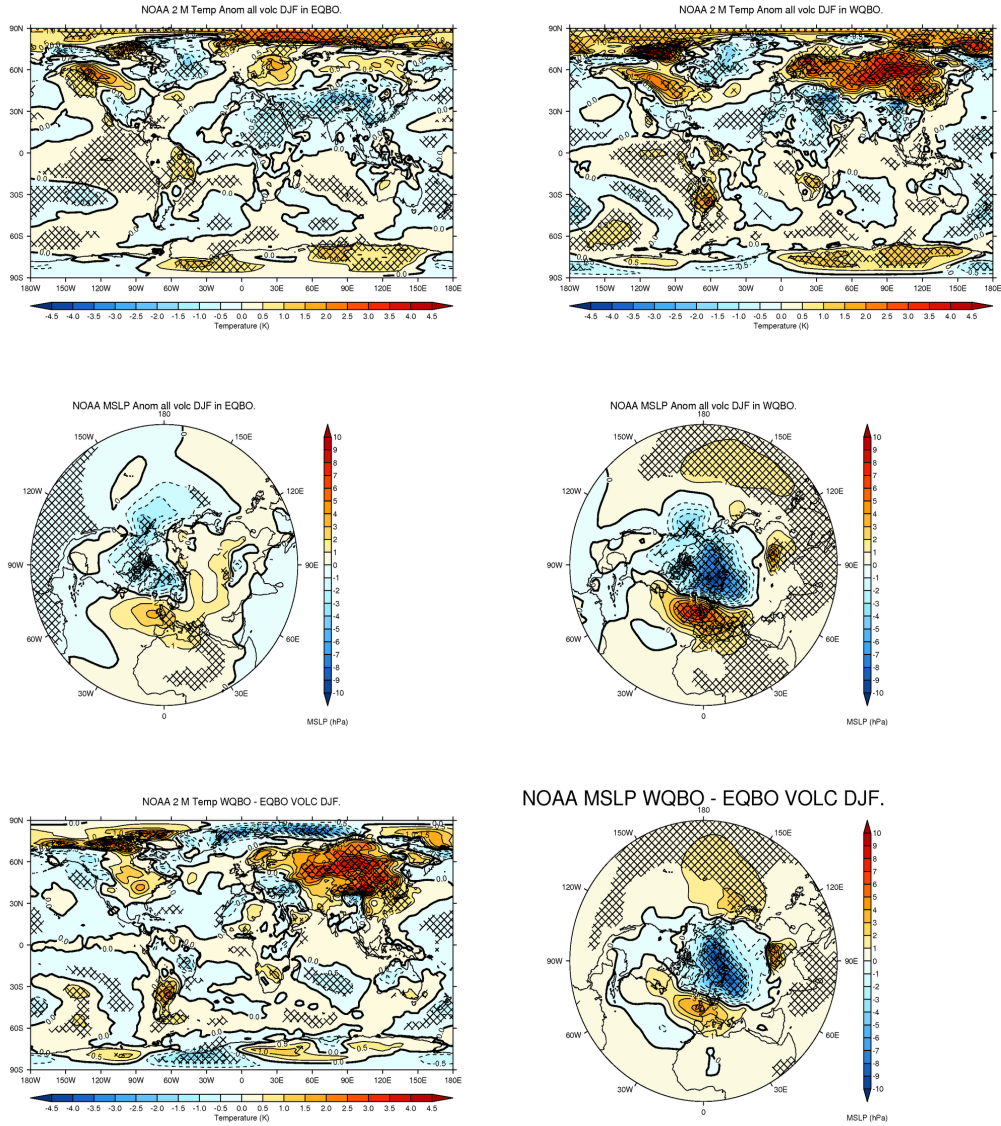


Figure 3.14: NOAA Composite Anomalies for East and West QBO Phase. First row displays 2 M temperature anomalies of all volcanic East QBO (left) and West QBO (right) winters from climatology. Third row displays MSLP anomalies of all volcanic East QBO (left) and West QBO (right) winters from climatology. Third row displays the difference plots of the West QBO field subtracted from the East QBO field for temperature (left) and MSLP (right). Hatching displays areas at or over 99 per cent significance using a Monte Carlo significance test.

subtracted from the East QBO 2 metre Temperature and MSLP fields) shown in figure 3.13 reveal statistically significant warm anomalies over Eastern North America and cool anomalies over the West Polar Pacific region and Far Eastern Russia in

west QBO phases, whilst MSLP fields reveal significant changes in pressure over North America and the Pacific which could be due to activation of the Pacific North American pattern..

Figure 3.14 shows the effects of the QBO on 2 M Temperature and MSLP for all volcanic winters split into the East or West phases of the QBO. The temperature fields reveal a huge impact of the phase of the QBO on the 2 M temperature anomaly fields. West QBO phase winters reveal a large statistically significant warming of up to 4K over almost all of Eurasia (using a Monte Carlo statistical significance test). We note that we choose the more computationally expensive Monte Carlo test over the standard t-test due to its suitability for being more robust for lower sampling numbers than a normal t-test. By separating into QBO phase the statistical significance has increased and figure 3.14 shows extensive areas of 99% significance that demonstrate the robustness of the signal. In the West QBO fields there exists significant Middle Eastern cooling synonymous with a strong positive NAO (Stenchikov et al. (2006)). However, in the Eastern QBO phase, there exists no statistically significant warming over Eurasia anywhere. We note this is an especially important point that is masked when composite anomalies over all years. The main Eurasian signal for East QBO winters is that of a statistically significant cooling further south, particularly over the India and China. MSLP fields reveal that volcanic winters in a West QBO phase also exhibit a significant positive NAO pattern in mean sea level pressure. The East QBO has a weak NAO which does not demonstrate the same statistically significant robustness. Figure 3.13 also shows difference plots of the West QBO volcanic winter fields subtracted from the East QBO fields. These reveal major differences in the Eurasian winter warming during the Westerly and Easterly QBO phase. MSLP fields also confirm that the NAO index is excited dependent on the QBO phase with a Westerly QBO phase causing a more positive NAO, with large values statistically significant at the 99% level over all of the NH polar region.

3.3 Precipitation and hydrological impacts of the positive NAO following an eruption

Previously, studies of volcanic eruptions have been more commonly focused on dynamical and radiative effects, with precipitation receiving relatively little focus (e.g. Robock and Mao [1992], Graf et al. [1993], Stenchikov et al. [1998], Timmreck et al. [1999], Stenchikov et al. [2002], Stenchikov et al. [2004], Stenchikov et al. [2006], Robock et al. [2007], Graf et al. [2007], Ottera [2008], Kravitz and Robock et al. [2011]). However, precipitation has extremely large impacts on agriculture (e.g. Rosenzweig and Hillel (1998)) and lack of sufficient access to water resources during the period following the Pinatubo eruption caused severe political tensions on some areas in the Mediterranean (Houston and Griffiths (2008)).

Changes to the climate's hydrological cycle can also, however, be caused by variability. Previous studies on more recent eruptions have been more focused on only Pinatubo (e.g. Trenberth and Dai (2007)), whilst modelling studies often are unable to reproduce the observed NH winter dynamical changes to volcanic eruptions (e.g. Stenchikov et al. (2006)). The dynamical influence of volcanic eruptions on precipitation has been suggested from analysis of proxy data to offset or even overwhelm radiative changes on precipitation in the Asian monsoon region (Anchukaitis (2010)).

Here, we present ERA40 analysis of anomalies in precipitation, runoff and PDSI (see Palmer (1965) and Dai et al. (2004) for further details and its calculation) following the past 4 major eruptions, as analysed in figure 3.8. The anomalies are that of 1 NH 'water year' following a volcanic eruption from climatology - the NH water year comprises one year starting at 1st October and ending on the 30th September, corresponding with the start of the season of soil moisture recharge, includes maximum runoff, and concludes with the season of maximum evapotranspiration (Trenberth and Dai (2007)). Not shown here were graphs calculated using the SH water year - defined analogously to the NH water year but for the SH, the SH water year is from 1st July to the 30th June. Little dependence on the choice of water year was seen.

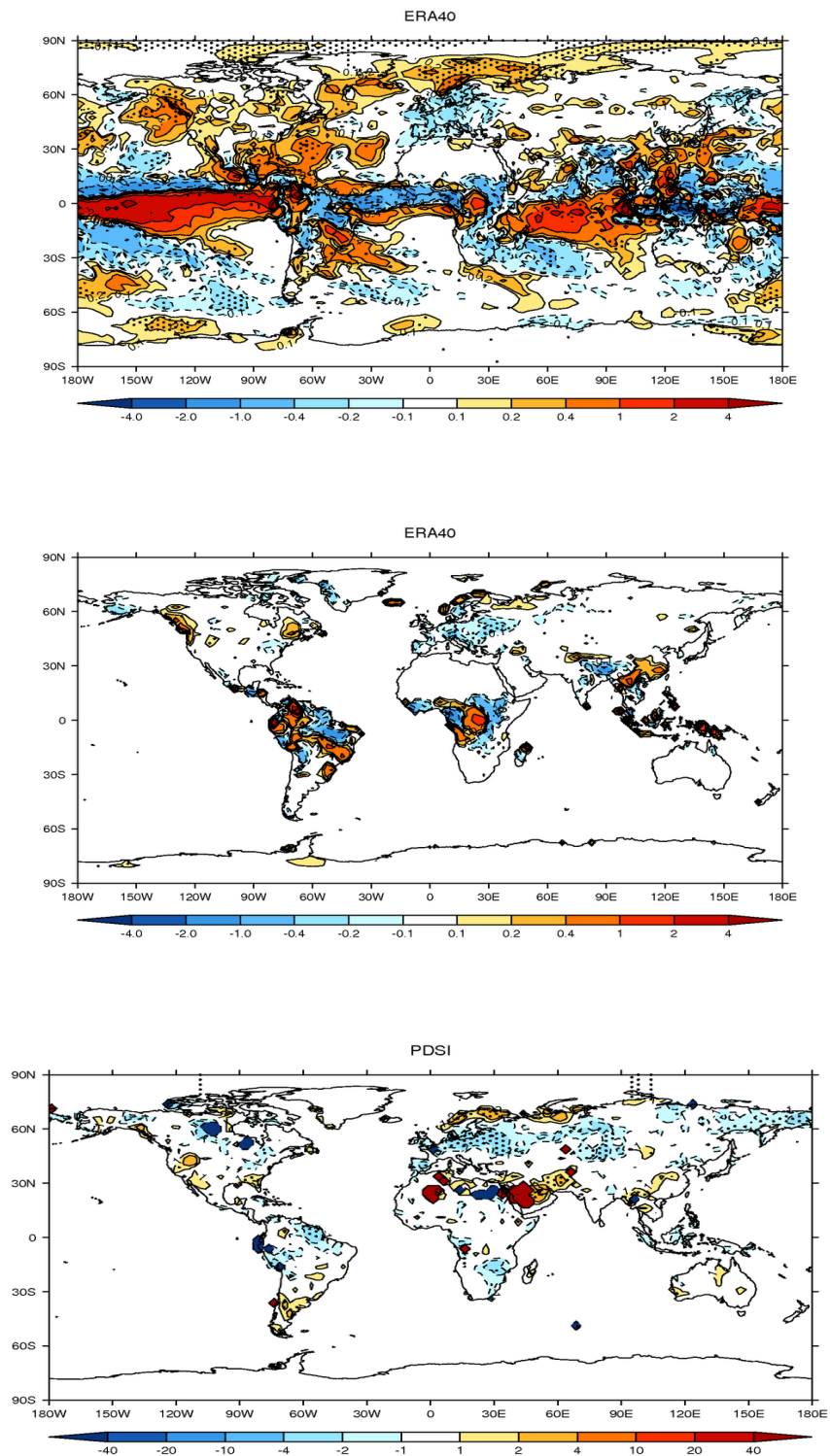


Figure 3.15: Precipitation (top row), runoff (second row) and PDSI composite anomalies (all in mm/day) for the past four major eruptions. Stippling displays areas at or over 95 per cent significance using a two tailed t-test.

Despite the high level of variability in precipitation and the small sample size figure 3.15 shows a statistically significant increase in Northern European precipitation with a corresponding decrease in precipitation. It is known that a positive AO/NAO the North Atlantic stormtracks also shift northwards, meaning Northern Europe becomes warm and wet, whilst Southern Europe becomes dry (Walter and Graf (2005)), however this is the first case demonstrating that volcanic eruptions can cause possible drought in Europe due to the strengthened stratospheric polar vortex and positive NAO that result from the increased temperature gradients caused by lower stratospheric aerosol heating. Such decreases over European land, accompanied with increases North of Europe could be indicative of more northerly Atlantic storm tracks due to a positive AO (recall figure 2.3). The large increase in precipitation in the tropical pacific ocean is likely due to El Nino of 1982/3 (Rasmusson and Wallace (1983)). Composite runoff anomalies shown in figure 3.15 reveal large decreases in runoff in Europe with slight but not significant increases at the northern-most region of Europe, consistent with precipitation patterns. The PDSI composite, which incorporates both the effects of precipitation and evaporation in a region, is consistent with the above analysis of precipitation and runoff. Large statistically significant decreases in PDSI are seen over all of mid and Southern Europe, whilst statistically significant increases in PDSI are seen over Northern Europe. The radiative forcing from a geoengineering scheme needed to restore the temperature of the Earth back to pre-industrial climate is comparable to the radiative forcing from Mount Pinatubo in many emissions scenarios (Vaughan et al. (*in prep/personal communication*)). These results here suggest possible adverse and unintended consequences arising from *dynamical* changes in the stratospheric polar vortex from sulphate aerosol geoengineering implementation. A further study that would allow for more ensembles and more robust statistics would be to assess precipitation changes in a model that could capture the NH winter dynamical response.

Chapter 4

Coupled Model Intercomparison Project 5 (CMIP5) simulations of climate following volcanic eruptions

4.0.1 Abstract

When sulfate aerosols are produced by volcanic injections into the tropical stratosphere and spread by the stratospheric circulation, it not only causes globally averaged tropospheric cooling but also a localized heating in the lower stratosphere, which can cause major dynamical feedbacks. Observations show a lower stratospheric and surface response during the following one or two Northern Hemisphere (NH) winters, that resembles the positive phase of the North Atlantic Oscillation (NAO). Simulations from 13 CMIP5 models that represent tropical eruptions in the 19th and 20th century are examined, focusing on the large-scale regional impacts associated with the large-scale circulation during the NH winter season. The models generally fail to capture the NH dynamical response following eruptions. They do not sufficiently simulate the observed post-volcanic strengthened NH polar vortex, positive NAO, or NH Eurasian warming pattern, and they tend to overestimate the cooling in the tropical troposphere. The findings are confirmed by a superposed epoch analysis of the NAO index for each model. The study confirms previous similar evaluations and raises concern for the ability of current climate models to simulate the response of a major mode of global circulation variability to external forcings. This is also of con-

cern for the accuracy of geoengineering modeling studies that assess the atmospheric response to stratosphere-injected particles.

4.0.2 Introduction

For a volcano to have a significant long-term impact on the climate it must inject a sufficient amount of sulfur containing gases into the stratosphere (?). Once in the stratosphere the sulfate gas undergoes a chemical reaction to produce sulfate aerosol. The e-folding time of the sulfate gas to particle conversion is typically 30-40 days (?). Sulfate aerosol scatters back to space the incoming shortwave radiation (SW) and also absorbs solar near infrared (NIR) radiation and upwelling long wave (LW) radiation from the surface and atmosphere below (???). For a given mass load, the scattering of SW radiation is modulated by the particle size distribution and as the aerosol particle size increases, scattering of incoming SW radiation decreases (?). The decrease in incoming shortwave radiation results in a cooling of Earth's surface (?). The typical e-folding lifetime for tropically injected volcanic aerosols is about 12-14 months (???), causing surface cooling for about two years following an eruption.

In contrast, localized equatorial heating, around 3 K for the Pinatubo eruption of June 1991 (?), occurs in the lower stratosphere due to the increase in absorption of NIR and LW radiation by the sulfate aerosols. For a tropical volcanic eruption the heating in the tropical stratosphere creates anomalous temperature and density gradients between the equator and poles. By the thermal wind relationship, this causes a strengthening of the zonal winds, which results in a strengthened stratospheric polar vortex. In addition, reduced surface temperatures in the tropical regions reduce the meridional surface temperature gradient, and this has been associated with a reduction in the Eliassen Palm (EP) Flux - essentially, a measure of planetary wave activity from the troposphere into the stratosphere (?) - and hence a stronger, less disturbed vortex. Further, chemical reactions which result in ozone depletion serve to cool and strengthen the vortex, and the reduced temperatures cause more NH ozone depletion, creating a positive feedback loop (?).

A substantial body of research has indicated an influence of the stratospheric vortex on high latitude circulations at Earth's surface, with a strengthened vortex

associated with a positive North Atlantic Oscillation/Arctic Oscillation (??????). The North Atlantic Oscillation (NAO) is an index corresponding to the difference in mean sea level pressure (MSLP) between the Azores and Iceland (??), and the Arctic Oscillation (AO) is defined as the first hemispheric empirical orthogonal function (EOF) of sea level pressure variability (??). Essentially the NAO can be thought of as the AO over the Atlantic region (?). A positive AO corresponds to anomalously low pressure over the pole, and anomalously high pressure at midlatitudes, and vice versa for the negative AO. After large volcanic eruptions a positive phase of the AO has been observed for the following 1 to 2 winters (??). The associated stronger westerly winds cause anomalous advection of warm oceanic air overland, and this results in anomalously warm temperatures over major NH landmasses (?). Thus, as a result of the combined result of the surface cooling and lower stratospheric tropical heating, a dynamical feedback occurs during NH winter, which results in surface warming over Northern America, Northern Europe and Russia (?). Negative surface temperature anomalies in the Middle East are also a distinctive feature of post-volcanic winters consistent with the positive phase of the AO (?, S06 hereafter) .

Climate model simulations of the historical period have, so far, been able to produce a slightly strengthened stratospheric vortex, but much weaker than the observations, and have failed to reproduce a positive AO and warming/cooling patterns over Eurasia and the Middle East respectively for the two NH winters following volcanic eruptions [S06]. S06 analyzed seven models used for the Fourth Assessment Report of the Intergovernmental Panel on Climate Change (?). They included all the models that specifically represented volcanic eruptions by including a layer of aerosol, and excluded those that either did not represent them, or represented them simply by a reduction in the solar constant. They found that the temperature increase in the lower equatorial stratosphere, caused by radiative heating from the aerosol, was reproduced by all the models. However, the models showed less agreement with the observed post eruption NH winter polar lower stratospheric cooling. Further, the 50 hPa polar geopotential height (indicative of the strength of the stratospheric polar vortex) in the models generally showed almost no change whereas the observations show a large negative anomaly of about 200 m, revealing a statistically significant stronger than

average polar vortex at the 90% level. Furthermore, the AO responses in the model simulations were significantly weaker than in observations, indeed, ? notes that some model simulations show no AO response. Correspondingly the strength and spatial pattern of the surface temperature anomalies were not well reproduced.

Since the previous analysis of S06, who used simulations from the the World Climate Research Programme's (WCRP's) Coupled Model Intercomparison Project phase 3 (CMIP3) multi-model dataset (?), climate models have undergone changes and improvements, and spatial and vertical resolutions have been increased. In this study, we repeat the analysis of S06 using model simulations from the Coupled Model Intercomparison Project phase 5, (CMIP5, (?)) and focus our analysis on the impact of the largest volcanic eruptions on the NH winter circulation. The models and experiments are described in section 2, results are presented in section 3, and in section 4 we present our discussion and conclusions.

4.0.3 Models and Experiments

The model runs analyzed in this study come from the historic simulations of the climate of the 20th century as standardized for the CMIP5. Models were forced with natural and anthropogenic forcings from the late 19th century to the early 2000s. Although the major external forcings (such as solar, greenhouse gases, land use) are standardized based on the most recent observational databases, no specific recommendations were issued for other forcings such as the stratospheric injection of sulfate aerosols from explosive volcanic eruptions. As for the CMIP3, most modeling groups imposed the stratospheric emissions for volcanic eruptions either from the reconstructions of ? (AM), its update ? (AM07), or from the updated version of ? (ST, updates available at data.giss.nasa.gov/modelforce/strataer). The AM dataset provides monthly latitudinal distributions of stratospheric optical depth for each volcanic event in 64 latitude bands, computed with an explicit representation of the spread of the aerosol cloud, taking into account the seasonal variations in stratospheric transport. A fixed particle size distribution is assumed for all eruptions, with spherical droplets of sulfuric acid of effective radius of 0.42 μm . AM, however, only extends back to 1890. An updated dataset AM07 provides data well before the

start of the historical simulations (1850) and many modelling groups use either AM07 or combine AM with ST to overcome this problem, as we detail for individual models in Table ??.

The ST dataset provides monthly latitudinal zonal mean stratospheric optical depths for 24 layers between 15 km and 35 km together with variations of the particle's effective radius based on the observations of the 1991 Mt. Pinatubo and 1982 El Chichón eruptions. In GFDL-CM3 model the optical characteristics were calculated following ? using the optical depths from ST dataset and its updates.

Unlike the other models, MRI-CGCM3 interactively computes the conversion from SO₂ amount to stratospheric aerosol. It includes the aerosol model MASINGAR mk-2 (?), which calculates five species (sulfate, black carbon, organic carbon, mineral dust, and sea-salt) of aerosols from emissions and other processes, including sulfate aerosol of volcanic origin. The aerosol model is interactively coupled with the atmospheric component that calculates radiation and cloud microphysics and utilizes the inventory of volcanic SO₂ emissions provided by ???? and the optical properties of spherical sulfate aerosol droplets provided by OPAC (Optical Properties of Aerosol and Clouds, (?)).

We restricted model analysis to those models that were both forced with volcanic aerosol in the stratosphere and had at least 2 ensemble members, which yielded a total of 13 different climate models. The models with a brief description of the basic characteristics are listed in Table ?. 3 models, GISS-E2-R, CCSM4 and GFDL-CM3, in their updated version, are common to both our analysis and that of S06.

Table ?? lists the nine major volcanic eruptions between 40°S and 40°N over 1883-present day as well as the anomaly period, the latitudes of eruption and the SO₂ injected in the lower stratosphere as reconstructed by ?????. Following S06 the eruptions listed in Table ?? are a subset of the volcanic events analyzed by ?. In the same approach as S06, high-latitude eruptions from those studied by Robock and Mao are not included because they appear to produce a qualitatively different effect on circulation than lower-latitude eruptions (????). The volcanoes listed in Table ?? also correspond to the volcanoes south of 40°N in ? with the caveat that we use different dates for the first winter after the eruptions of Santa María and Fuego, shifting them

forward one year with respect to Christiansen's convention. The implication of this choice is explored in section 3.4.

Table 4.1: Models used in the study and their basic characteristics (horizontal resolution, vertical levels and model top), imposed aerosol forcing and number of ensemble members available. In the last column are listed the variables analysed for each model (T=1.5 m temperature, P=mean sea level pressure, Z=geopotential height).

Model Name	Modeling Group	Atmospheric Resolution	Model Top	Volcanic Forcing	N. of ens. members	Variables
bcc-csm1.1 ^a	Beijing Climate Center, China Meteorological Group	T42L26	2.9hPa	?	3	T,Z,P
HadGEM2-ES ^b	Met Office Hadley Centre	1.25°Lat x 1.875°Lon L38	3hPa	?	4	T,Z,P
HadCM3 ^c	Met Office Hadley Centre	2.5°Lat x 3.75°Lon L19	5hPa	?	10	T,Z,P
CanESM2 ^d	Canadian Centre for Climate Modelling and Analysis	T63L35	1hPa	?	5	T,Z,P
CNRM-CM5 ^e	Centre National de Recherches Meteorologiques / Centre Europeen de Recherche et Formation Avancees en Calcul Scientifique	T127L31	10hPa	?	10	T,Z,P
GISS-E2-H ^f	NASA Goddard Institute for Space Studies	2°Lat x 2.5°Lon L40	0.1hPa	?	5	T,Z,P
GISS-E2-R ^f	NASA Goddard Institute for Space Studies	2°Lat x 2.5°Lon L40	0.1hPa	?	5	T,Z,P
NorESM1-M ^g	Norwegian Climate Centre	0.9°Lat x 1.25°Lon L26	2.9hPa	?	3	T,Z,P
CCSM4 ^h	National Center for Atmospheric Research	0.9°Lat x 1.25°Lon L26	2.9hPa	?	6	T,Z,P
CSIRO-Mk3-6-0 ⁱ	Commonwealth Scientific et Industrial Research Organization with Queensland Climate Change Centre of Excellence	T63L18	10hPa	?	10	T,Z,P
MRI-CGCM3 ^l	Meteorological Research Institute	T159L48	0.01hPa	interactive**	3	T,Z,P
MPI-ESM-LR ^m	Max Planck Institute for Meteorology	T63L47	10hPa	?	3	T,Z,P
GFDL-CM3 ⁿ	NOAA Geophysical Fluid Dynamics Laboratory	C48L48	0.01hPa	? and ?	5	T,Z,P

The references for each model are: a) ? and ?, b) ?, c) ?, d) ?, e) ?, f) ?, g) ? and ?, h) ?, i) ? l) ? and ?, m) ?, ?, n) ?

^aThe Ammann et al. [2003] dataset spans the period 1890-1999. bcc-csm1.1 uses updates by ammann in 2004 to cover 1870-1999 combined with Sato. Et al. [1993] for the period 1850-1869

**From stratospheric SO₂ injection data from ?, ?, ?, and ?

Table 4.2: Major low latitude eruptions over 1883 to present day.

Volcano	Eruption Date	Latitude	Winters Analyzed		Reference Period	Lower Strat. SO_2 mass (Tg)*
Krakatau	Aug 27, 1883	6.10°S	1883-1884	1884-1885	1860-1882	44
Tarawera	Jun 10, 1886	38.23°S	1886-1887	1887-1888	1860-1882	4-5
Bandai	Jul 15, 1888	37.60°N	1888-1889	1889-1890	1860-1882	3-4
Santa María	Oct 24, 1902	14.76°N	1903-1904	1904-1905	1890-1901	30
Quizapu	Apr 10, 1932	35.65°S	1932-1933	1933-1934	1915-1931	3
Agung	Mar 17, 1963	8.34°S	1963-1964	1964-1965	1934-1955	20
Fuego	Oct 10, 1974	14.47°N	1975-1976	1976-1977	1965-1973	4
El Chichón	Apr 4, 1982	17.36°N	1982-1983	1983-1984	1976-1981	7
Pinatubo	Jun 15, 1991	15.13°N	1991-1992	1992-1993	1985-1990	20

*From stratospheric SO_2 injection data from ?, ?, ?, and ?

For comparison with observations the reanalysis of the 20th Century version 2 (20CRv2, (?)) is employed. From this dataset we will use only near-surface temperature and Mean Sea-Level Pressure (MSLP) fields for the period of 1871 to 2008. Our results compare similarly across a number of observational reconstructions such as HadCRUT2v and HadSLP1 (used in S06), and so the choice of product does not alter our conclusions. More information about the database is provided at <http://www.esrl.noaa.gov/psd/>. The ERA40 (?) and NCEP/NCAR (?) reanalysis fields are also used to compare with middle atmosphere circulation changes during the winter season for the largest eruptions after 1950.

To isolate the anomalies of the post-volcanic seasons and generate the average volcanic composite, we adopt the same averaging procedure employed by S06, choosing a different reference time for each eruption and averaging two winter seasons after each eruption. The statistical significance of anomalies from the mean climatology is evaluated with a local two-tailed t-test. We also compute the multi-model mean of the post-volcanic anomalies averaging with equal weight the ensemble mean of each model. All model have been interpolated to a common $2.5^{\circ}\text{Lat} \times 3.75^{\circ}\text{Lon}$ grid.

Using a large number of eruptions and minimum of two ensemble members per model (lending an equal weight to each ensemble member in the computation) should help to average out spurious effects, for example due to incorrect sampling of the El Niño Southern Oscillation (ENSO) cycles, which cannot be controlled in these coupled ocean atmosphere simulations. However, we also calculate the 3.4 ENSO index for each model (Table ??) by computing the area averaged total SST from the Niño 3.4 region, computing the monthly climatology (1950-1979) for area averaged total SST from the Niño 3.4 region, and subtracting the climatology from the area averaged total SST time series to obtain anomalies. These anomalies are then smoothed with a five-month running mean, and then normalized by the standard deviation over the climatological period (1950-1979).

? showed through analysis of observations that the largest volcanic eruptions of the 20th Century tend to be followed by a positive index of the North Atlantic Oscillation (NAO). He noted that the NAO signal is strongest and significant in the

first year after the eruption and does not appear to be influenced by ENSO events or by the specific volcanic eruption chosen for the composite.

We computed the NAO index for each model and each ensemble member to test whether the simulated dynamical response to volcanic forcing projects onto the NAO index as observed by ? in the observations. The NAO index is computed for each ensemble member of each model, as in ?. We first compute the Empirical Orthogonal Functions (EOFs) of the monthly winter (DJF) MSLP anomalies north of 20°N and between 110°W and 70°E for the period 1948-2000. Each pressure data point is weighted by the square root of the grid area it represents, consistent with ?. The seasonal winter (DJF) NAO index is computed from the monthly indices, defined as the principal component of the monthly anomalies of the MSLP projected onto the first EOF for the total period 1860-2000 and normalized to unit variance. The same index is computed for the 20CRv2 MSLP data. The EOF pattern for each model is shown in Fig. ??

We compare models and reanalysis using a superposed epoch analysis of the winter NAO (DJF) for the nine volcanic eruptions listed in Table ???. We take the winters in the neighboring ten years close to the first winter after each eruption (five years before and five years after) as defined in Table ??? and generate an “eruption matrix” whose rows represent each eruption event. The eruptions in each ensemble member are considered to be independent events, hence the number of rows in the “eruption matrix” is different for each model because it depends on the number of ensemble members. The rows are then averaged to obtain the epoch composite of 11 years, from winter in year -5 to winter in year +5 with year 0 the first winter after an eruption.

The statistical significance of the epoch analysis is estimated using the bootstrap method (?). We reshuffle with replacement the elements of each row to generate a new “random eruption matrix” and average the rows into a new epoch composite. The procedure is repeated 5,000 times obtaining a distribution of NAO values for each lag of the epoch composite. The random composites are drawn from the original epoch matrix to preserve the structure of the sample. We also adopted the normalization procedure described in ? to avoid possible biases due to single outliers in each volcanic window, but the main conclusions are not affected by the normalization. We compare

the level of the NAO index for each year of the composite with the 5%-95% and 1%-99% percentile levels of the bootstrap distribution.

We also tested for the occurrence of positive NAO for both in the first and second post-volcanic winter and its significance is tested using a bi-nomial distribution with the probability of the single event (σ) estimated from the full timeseries. As noted in ?, σ is in general different from 0.5 which is due to the probability distribution of the NAO index not being normal. σ for each model is reported in Fig. ?? and ??.

The main conclusions are robust with respect to the definition of the winter season (DJF or DJFM) and we will present here the results for the NAO index computed for the DJF composite to allow comparison with previous results in the literature.

4.0.4 Results

4.0.4.1 Direct radiative effect of volcanic aerosol

Due to a lack of direct information on the radiative forcing of volcanic aerosol for each model, we choose to use the time series of the anomalies in the reflected short wave (SW) radiation at the top of atmosphere (TOA) (Fig. ??) as a rough proxy for the global radiative effect of the stratospheric aerosol, as in S06 (their Fig. 1). All the models perform consistently with each other and show the increase in the reflected SW radiation corresponding to the major explosive eruptions and do not show any appreciable differences compared with the CMIP3 models shown in S06. The largest anomaly in the reflected SW radiation is observed for the bcc-csm1-1 model whereas MRI-CGCM3 simulates the lowest signal among the models. MRI-CGCM3 computes interactively the effect of the volcanic aerosol from the stratospheric SO₂ load and shows a lower scattering efficiency of incoming SW radiation with respect to the other models, even in the satellite-constrained era. This is possibly due to the interactive chemistry conversion processes affecting the properties of the aerosol created from the SO₂ in the lower stratosphere. Large differences between this model and other all other models, forced by imposed changes in lower stratospheric optical depths, raises questions about the realism of the MRI model with regards to the TOA anomalies.

As noted in S06, larger spread among the model response is observed for the early eruptions and less uncertainty appears for the most recent El Chichón and Pinatubo

events. Notably, the largest effect on the reflected SW radiation for the eruptions pre-1900 is observed in the models that adopt the AM reconstruction.

As a measure of the anomalous heating forced by the volcanic aerosol in the lower stratosphere, we analyzed the anomalies in the de-trended 30°S-30°N, 50 hPa temperature. Fig. ?? shows that the models simulate an increase in in the lower stratospheric temperature of about 2 K, up to 4 K for the largest eruptions of Pinatubo and Krakatau. The largest temperature anomalies are simulated by the models using the AM database, with heating for the Pinatubo eruption up to 10 K for CCSM4 and 7 K for NorESM1-M. MRI-CGCM3 shows anomalies close to the multi-model mean and generally larger than observed for the models using (?) database, but places the peak of the warming associated to the eruption of Agung about one year later than the other models.

The multi-model mean appears in good agreement with the temperature anomalies from the ERA40 reanalysis for the eruptions after 1960. The overestimation of the warming associated to Pinatubo is likely in part due to the cooling effect of the easterly phase of the QBO in the winter 1991-1992 (??), not accounted for in the CMIP5 models.

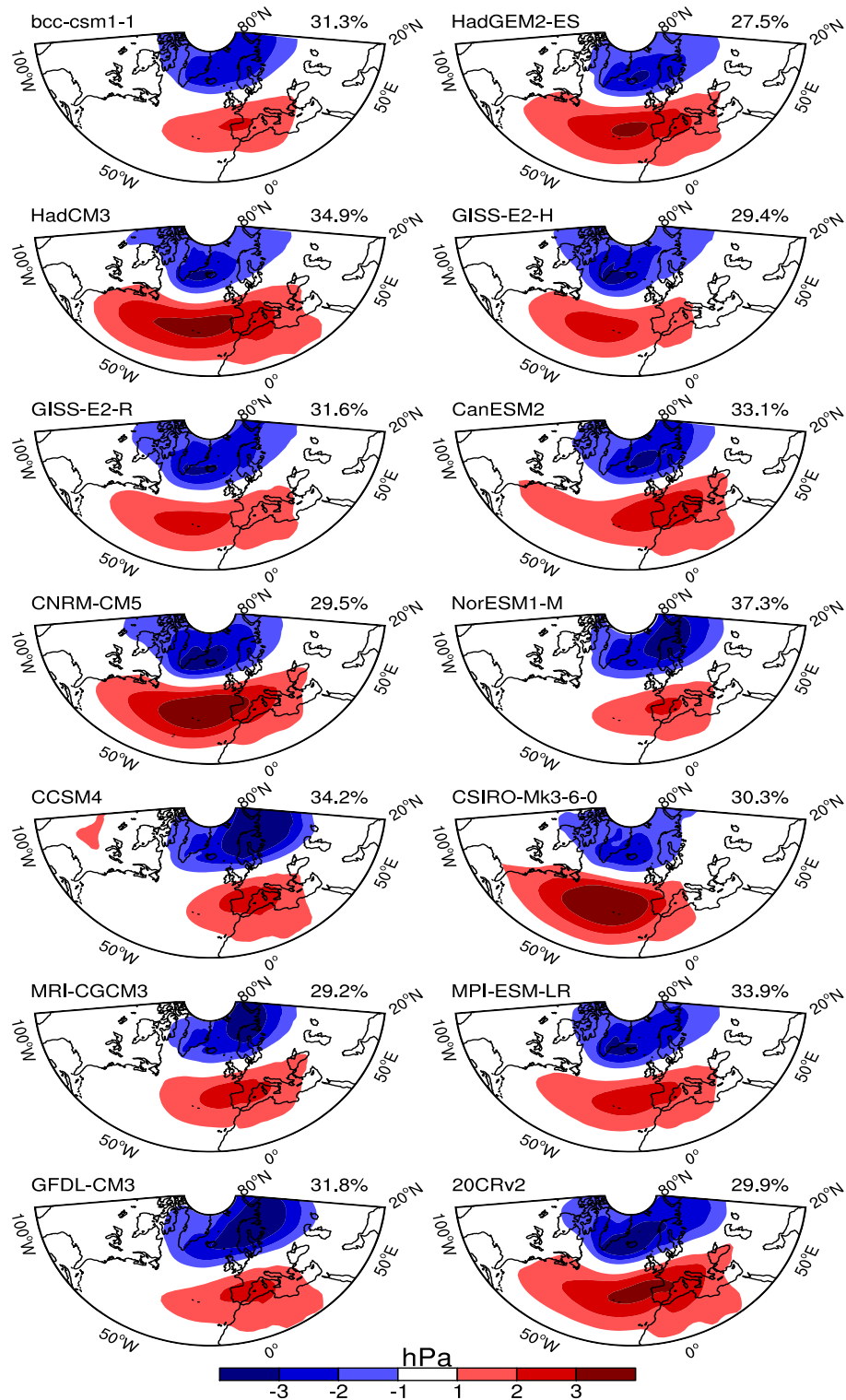


Figure 4.1: Leading EOF of the monthly winter (DJF) mean sea level pressure anomaly over the North Atlantic region (110°W-70°E) for each model ensemble mean and 20CRv2 over the period 1860-2000. EOF values are expressed as hPa. In the top right corner of each plot is indicated the percentage of variance explained by the first EOF.

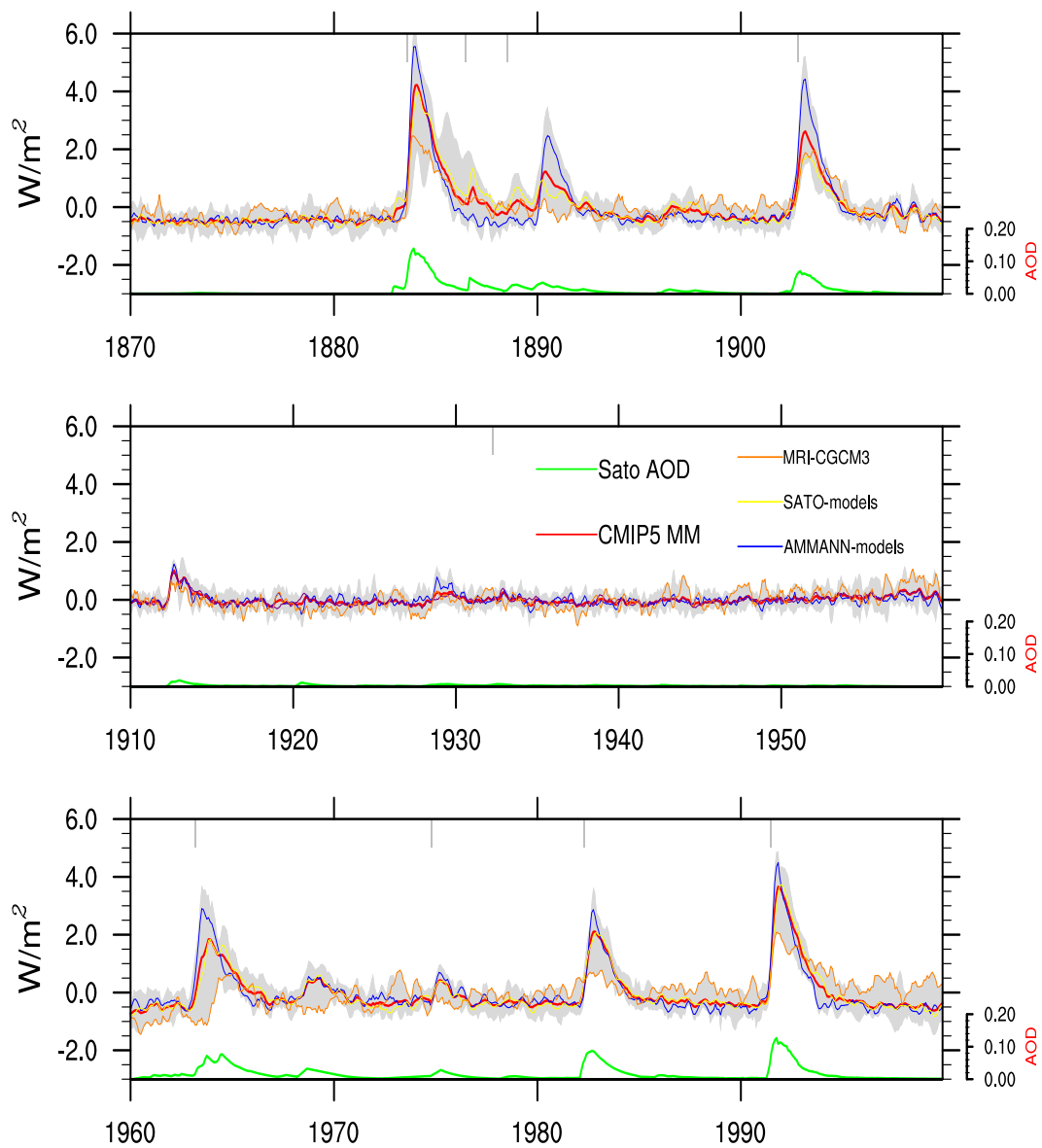


Figure 4.2: 3-months running average of global averaged de-trended and de-seasonalised TOA outgoing shortwave radiation anomalies for the 13 CMIP5 models listed in Table ??, over the period of 1860-2000. The gray shading shows the spread among the minimum and maximum of the means of each model ensemble. The lines show the multi-model mean (CMIP5-MM) and the multi model mean for the models using (?) database and (?). We show separate the ensemble mean for MRI-CGCM3, which computes interactively the evolution of volcanic aerosol. The green line at the bottom shows the 30°S and 30°N volcanic aerosol optical depth (AOD) at 550 nm from ? (and updates). The grey bars at the top of plots indicate the occurrence of the 9 volcanic eruptions listed in Table ??.

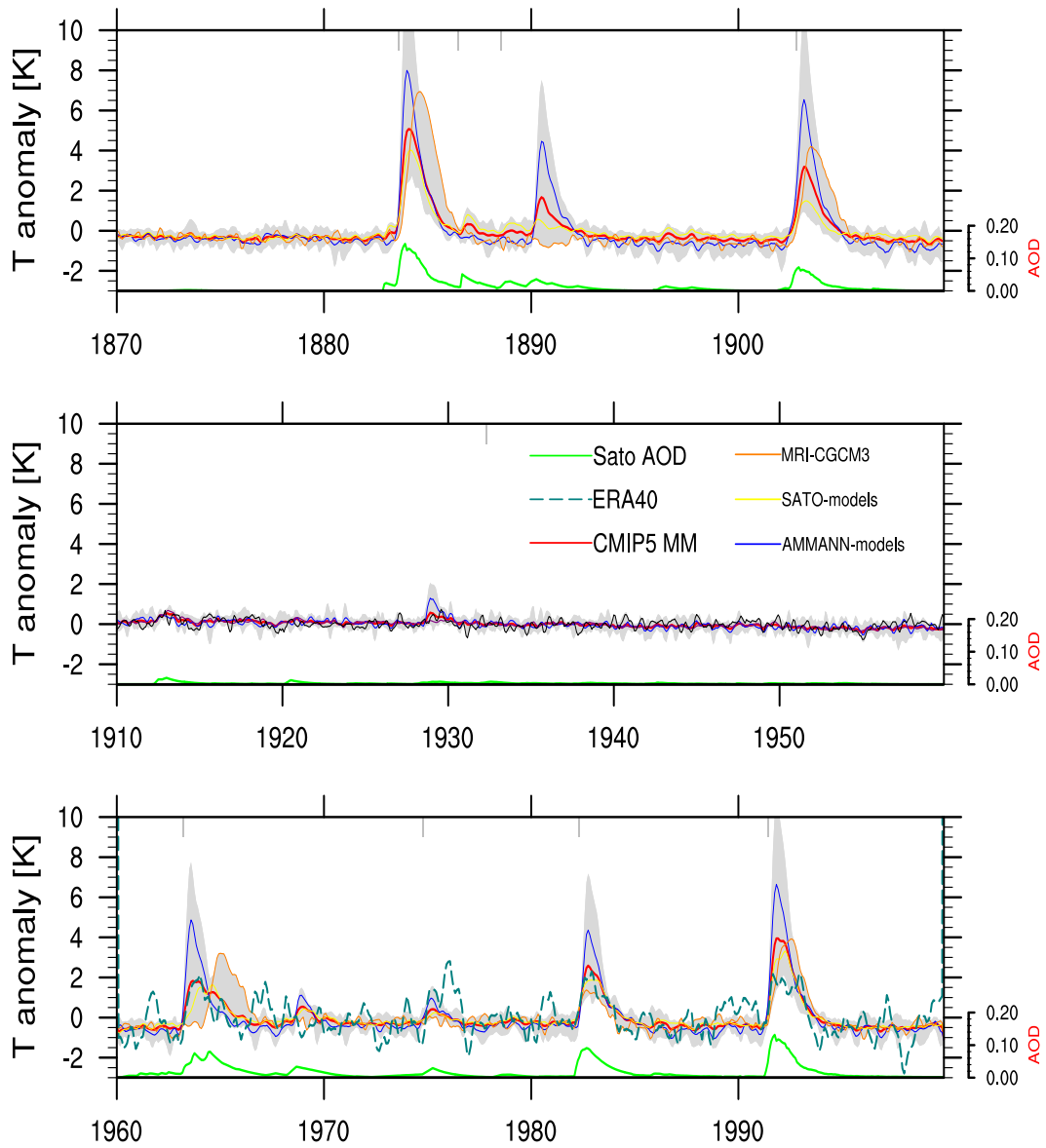


Figure 4.3: As Fig. ?? but for the 50 hPa temperature anomalies averaged between 30°S and 30°N. In the bottom panel the corresponding 50 hPa temperature anomalies from ERA40 are included.

4.0.4.2 Surface temperature and mean sea level pressure

Fig. ?? shows the NH composites of surface temperature, mean sea-level pressure (MSLP) and geopotential heights for the observations and the multi-model mean. We first focus on the surface temperature and MSLP for the post-volcanic winter season (as given in the fourth column in Table 2). Fig. ??a shows in the reanalysis the well known significant surface warming signal over northern Europe and Asia, where anomalies reach up to 2 K. Significant cooling is observed over NE America and also, though not significant, over the Middle East. As noted in S06, a warming signal also appears on the Eastern Pacific but this could be spurious due to a positive ENSO sampling bias. A general cooling is observed in the Tropical region, although weak and barely significant. The reanalysis surface temperature anomaly in the Arctic region appears unusually warm, but the reliability of the reconstructed lower tropospheric temperature at high latitudes reduces the significance of the anomaly (?).

The observed surface temperature anomalies in the NH post-volcanic winters are closely related to changes in the winter circulation as confirmed by the MSLP anomalies (Fig. ??c). In agreement with previous studies (e.g., S06), in the reanalysis a significant positive NAO-like pattern marks the North-Atlantic region, with negative pressure anomalies in the Arctic region and positive over the North-Atlantic. Notice that the minimum and maximum of the anomaly are both displaced northward with respect to the pattern of the leading mode of variability in the MSLP anomalies in the region as observed in Fig. ?? for the 20CRv2.

The multi-model aggregate of surface temperature and MSLP shows no such pattern (Fig. ??b,d). A general cooling is observed in the surface temperature anomaly field, however no dynamical response to a large tropical volcanic eruption can be seen in the multi-model aggregate. Fig. ??a,b reveals large areas of significantly different temperature and MSLP between the observations and models, especially over areas associated with the positive NAO and DJF surface warming.

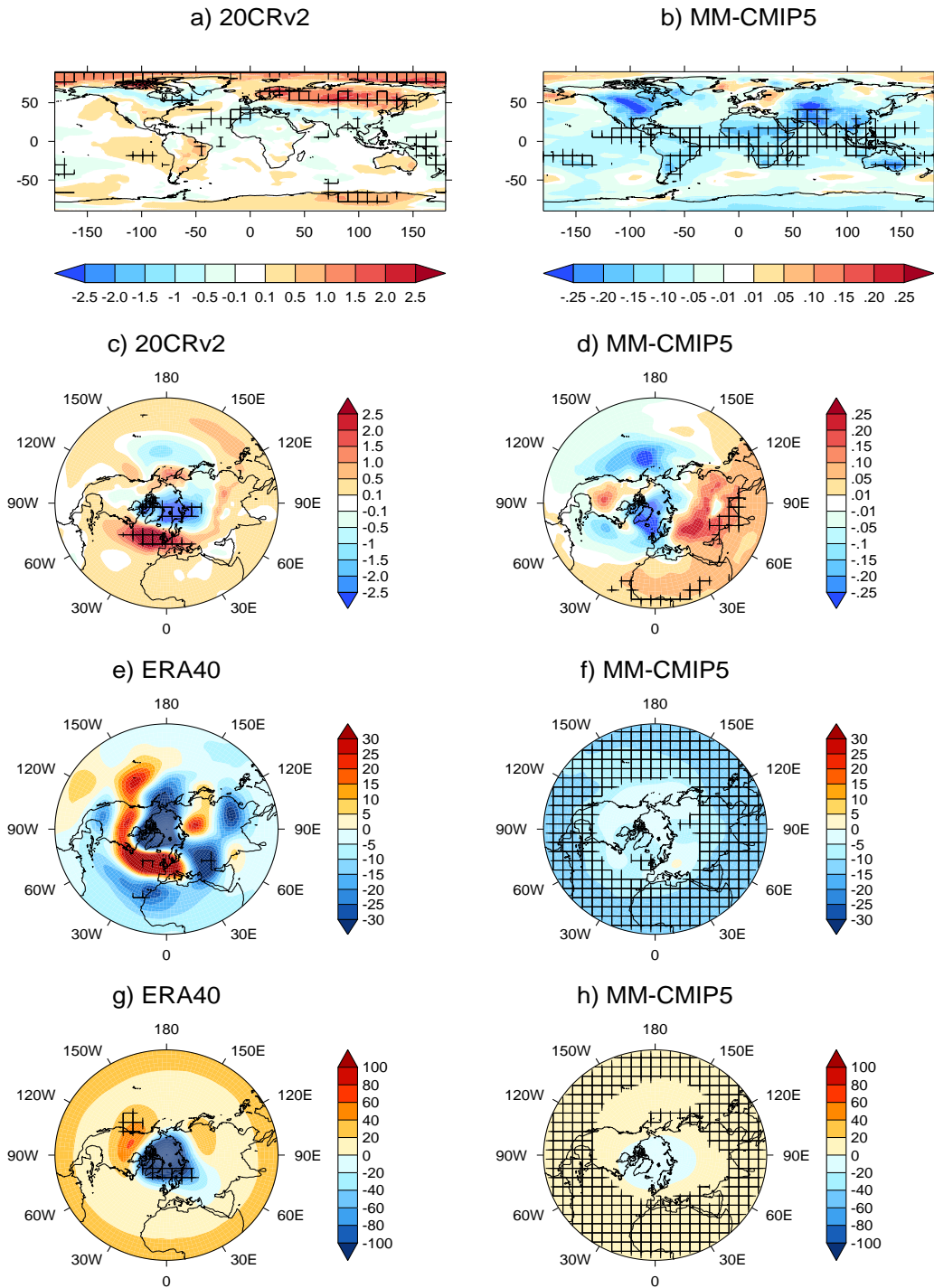


Figure 4.4: Comparison between reanalysis and multi-model mean. Composite anomaly averaged after 2 post-volcanic winters for (a,b) near-surface temperature (K), (c,d) mean sea level pressure (hPa), (e,f) and (g,h) respectively 200 and 50 hPa geopotential (m). The anomalies in (e,g) are computed for the last 4 volcanoes listed in Table ???. Hatching displays, for the left column areas at or over 95% significance using a local two tailed t-test, for the right column where at least 90% of models agree on the sign of the anomaly. Notice the different scale in (a,b) and (c,d)

Fig. ?? and ?? shows the NH composites of surface temperature and MSLP for the post-volcanic winter season in the individual models. Large variability is observed between the models in their NH response: the observed warming in the northern Eurasia is simulated by a few models but is much weaker than in the observations. For example, GISS-E2-H and GISS-E2-R simulate the northern European warming pattern reasonably well but the maximum amplitude is only 0.5 K. The cooling over NE Canada seems to be simulated more widely, independent of how well the northern Eurasian warming is captured. Some models (CSIRO-Mk3.6, HadGEM2-ES, NorESM1) simulate a general cooling in the Asian-European area, opposite to the observations, and the majority show a significant cooling in the tropical lower latitudes, of around 0.2K over the oceans.

Large inter-model differences in MSLP pattern are shown in Fig. ?. Only CNRM-CM5 and CanESM2 reproduce a weak dipole over the North-Atlantic, whereas NorESM1 shows anomalies opposite to those observed. The other models only show weak anomalies with minimal statistical significance. The two GISS models simulate weak surface temperature anomalies but do not show any significant anomaly in the MSLP. The GISS-E2-R model differs from GISS-E2-H in that its response is weaker, and not statistically significant. The only difference between the GISS-E2-H and GISS-E2-R models is the ocean model to which the atmosphere is coupled. GISS-E2-R uses the ModelE atmospheric code and is coupled to the Russell ocean model ($1^\circ \times 1.25^\circ$ L32), whilst GISS-E2-H uses the same ModelE atmospheric code but is coupled to the Hycom ocean model ($1^\circ \times 1.25^\circ$ L26) (?). In a modelling study on the effects of volcanic eruptions on the oceans ? reported changes in sea level, temperature, ocean heat content, salinity, and also significant strengthening of the Atlantic Meridional Overturning Circulation (AMOC) $40 - 60^\circ\text{N}$ in the first few years following an eruption. Whilst it is therefore possible that part of the surface response could be due to changes in NH ocean circulation, it is generally believed for AMOC changes, in particular, to be caused by the changes in wind stress due to positive NAO (?) that is a result of a stronger vortex following volcanic eruption (?), not that the ocean affects the surface to cause a positive DJF warming for up to two years following a volcanic eruption. Therefore it is unlikely that the response witnessed in

GISS-E2-H which differs slightly to GISS-E2-R, particularly with no strong positive NAO, is due to an activation of the volcanic mechanism.

The analysis of surface temperature and MSLP in the CMIP5 ensemble shows a poor correspondence with observations during the first two NH winters following large tropical eruptions. No improvement is seen with respect to the findings of S06 based on a selection of seven models participating in CMIP3.

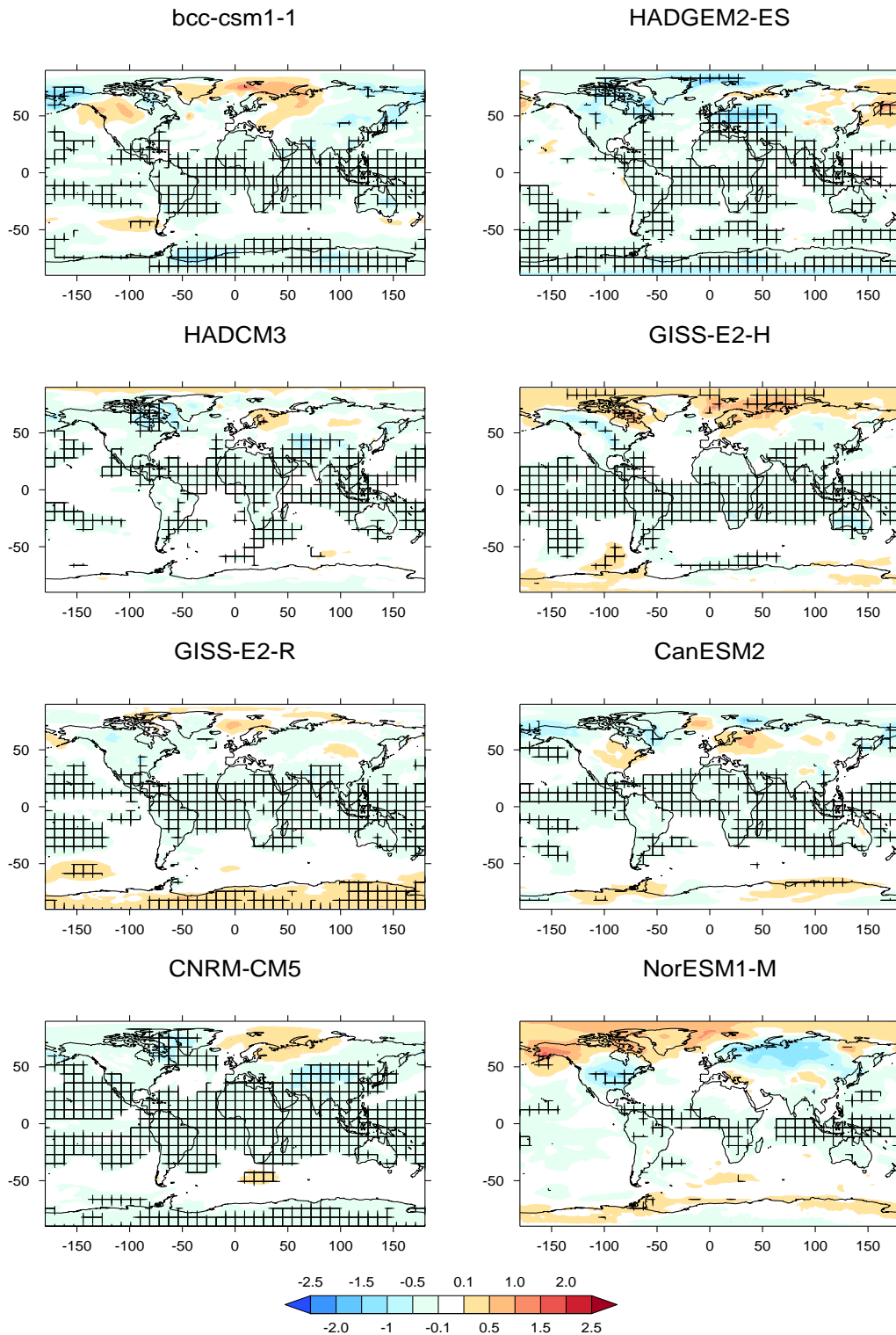


Figure 4.6: Composite near-surface temperature anomalies (K) for the two following winters of the past nine most recent large tropical volcanic eruptions (Table 2) in all models and the 20th century reanalysis (20CRv2). Hatching displays areas at or over 95% Significance using a two tailed t-test.

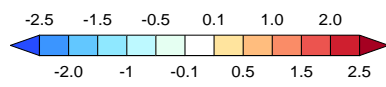
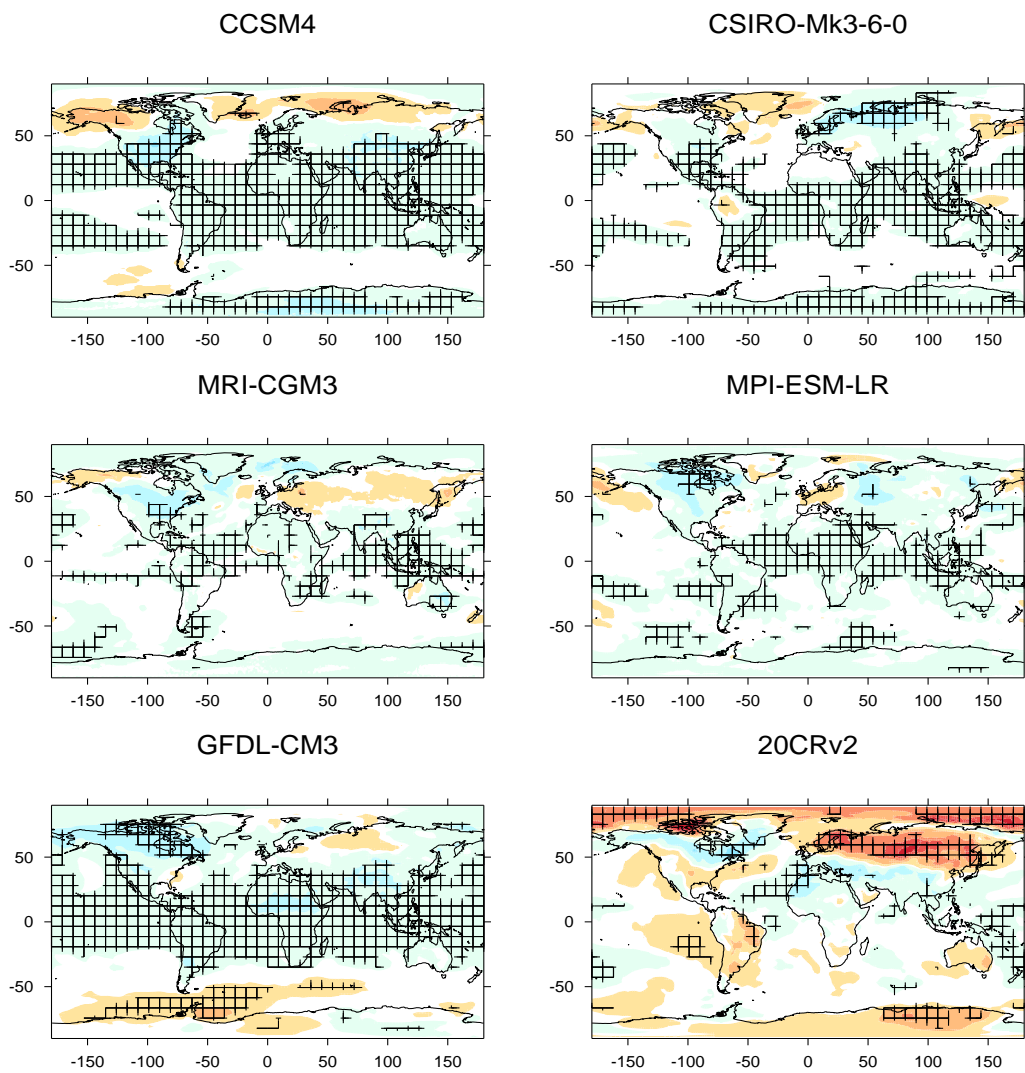


Figure 4.6: (continued)

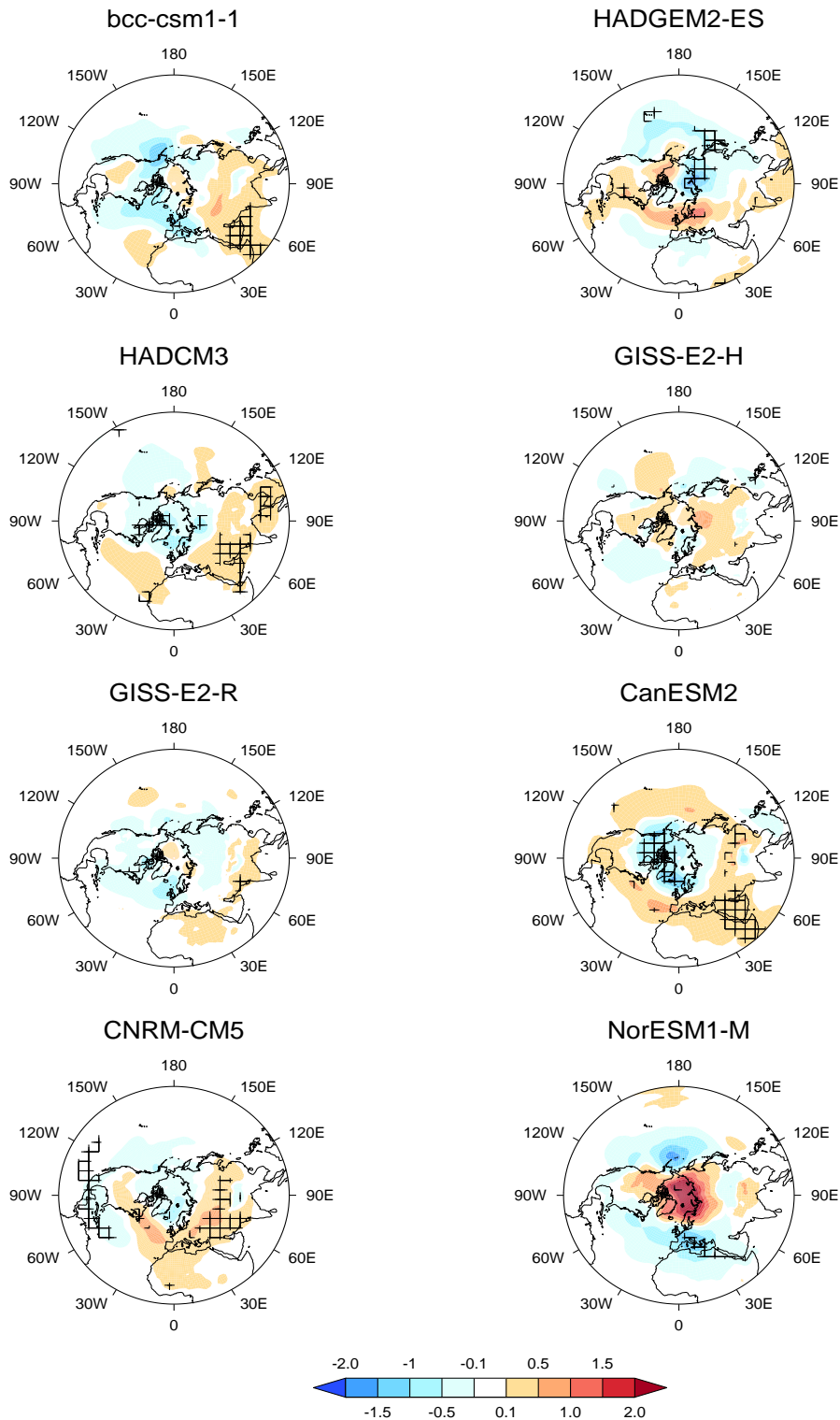


Figure 4.7: NH stereographic plot of composite MSLP anomalies (hPa) for the two following winters of the past nine most recent large tropical volcanic eruptions in all models and the 20th century reanalysis (20CRv2). Hatching displays areas at or over 95% Significance using a two tailed t-test.

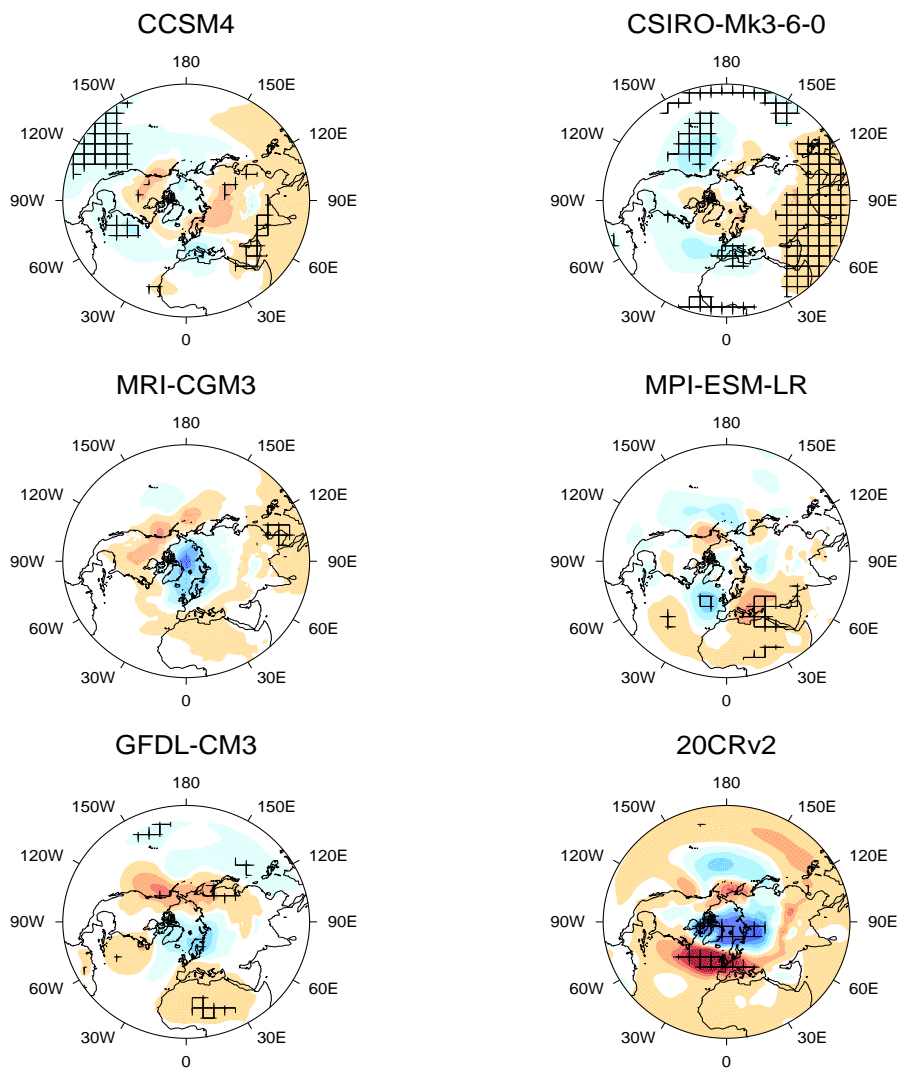


Figure 4.7: (continued)

4.0.4.3 Geopotential Height

Geopotential height anomalies in the upper troposphere and mid stratosphere help define circulation changes during winters following large volcanic eruptions. Due to the high uncertainty in the 20CRv2 reconstructions of upper air fields (?), we decide to analyze only the last four eruptions since 1950 using the ERA40 dataset. In the upper troposphere (Fig. ??e), the observed 200 hPa geopotential height anomalies are linked to the MSLP anomalies, with a general decrease over the North Pole surrounded by positive geopotential height in the mid latitudes and a strong dipole over the North Atlantic region. A general decrease in the observed geopotential height dominates at low latitudes, consistent with the generalized cooling tendency observed in the tropical troposphere.

In observations the anomaly pattern in the troposphere is mirrored in the stratosphere by a cold and deep polar night vortex, as observed in the 50 hPa geopotential height anomalies (Fig. ??g) showing a large statistically significant decrease in geopotential height over the pole of around 200 m. A weaker anomaly at 50 hPa is observed at low latitudes, with a geopotential height increase of about 25 m which has been attributed to the direct heating effect of the volcanic aerosol in the lower tropical stratosphere (??). The observed low 50 hPa geopotential height at high latitude is associated with a colder polar lower stratosphere, which suggests a stronger and persistent polar vortex. Recent studies suggest that this might be a characteristic of the early stage of the post-volcanic winter season. For example, ? saw no clear weakening of the wave activity during post-volcanic winter in observations and ? show that the observed polar vortex in the upper stratosphere is weaker than normal from the end of January into February after the three major volcanic eruptions since 1960.

As for the MSLP, the modeled geopotential height anomalies at 200 hPa are highly variable (Fig. ??). Most models simulate a significant uniform decrease in the geopotential height roughly south of 30°N, as can be seen in the multi-model composite Fig. ??f, stronger than in the observations. The strongest anomaly is observed for GFDL model. A significant uniform decrease over the Pole is observed only for MRI.

A few of the models capture the anomalies observed in the stratosphere (see Fig. ??) as in the reanalysis, though much weaker. HadGEM2, MPI, CNRM-CM5 and MRI simulate a decrease in the geopotential height of order of 25 m, although such a response is not a substantial change with regards to the background variability of the polar vortex. ? noted that over 1958-1997, as observed in ERA40, the leading EOF of 50 hPa wintertime geopotential height anomalies, which accounts for about 50% of the variance, is around -270 m. Other models show no significant anomaly at high latitudes. As observed from the multi-model mean Fig. ??h, the most robust feature in the stratosphere is a statistical significant increase in the geopotential height at low latitude in agreement with the observations. This is weaker than in the ERA40 composite (see Fig. ??d) and is likely due to the stronger cooling simulated in the tropics (Fig. ??b) which tends to shrink the atmospheric column, as noted in S06.

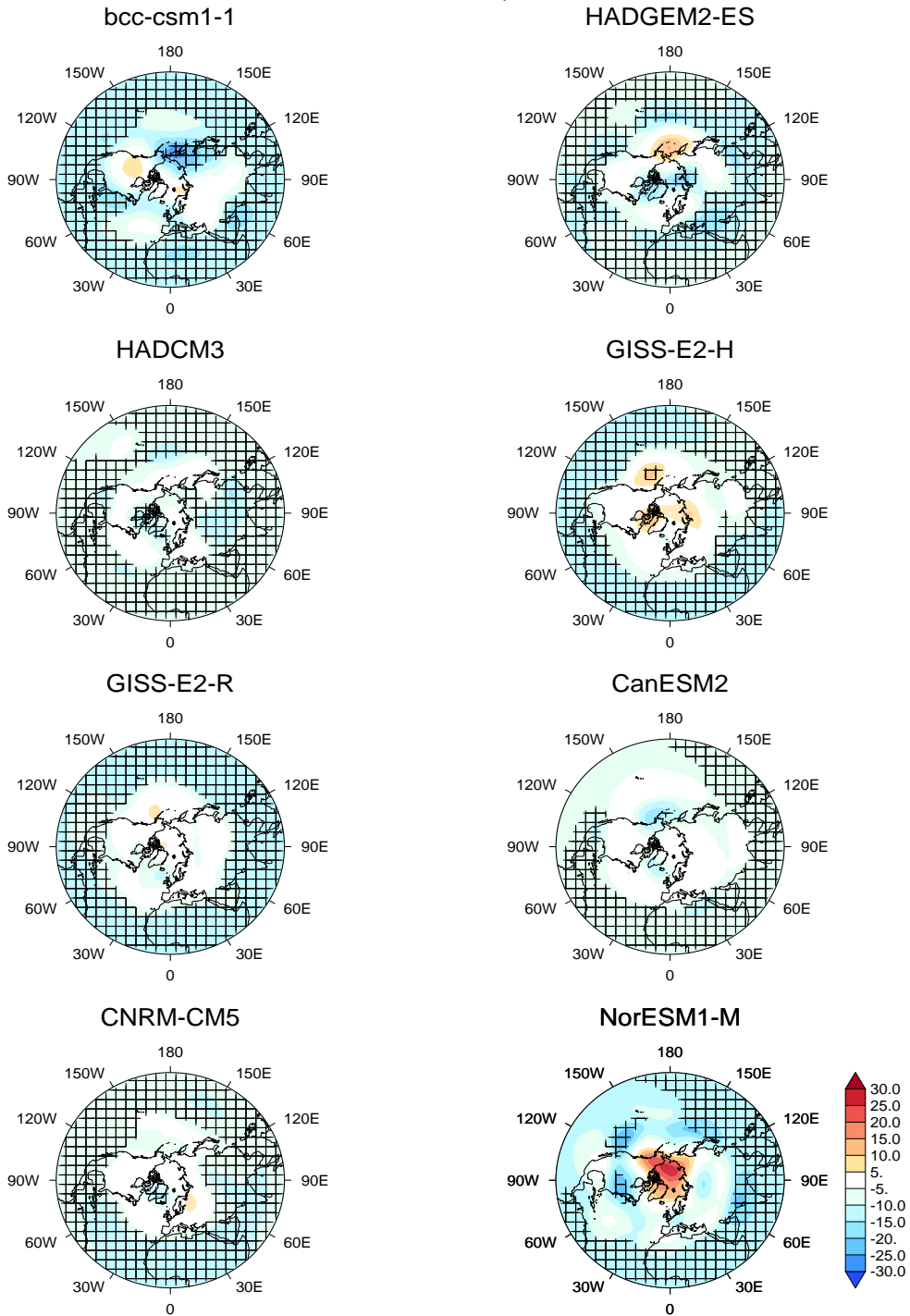


Figure 4.8: NH stereographic plot of composite 200 hPa Geopotential Height anomalies (m) for the two following winters of the past nine most recent large tropical volcanic eruptions in all models and ERA40 reanalysis. The anomalies in the reanalysis are computed for the 4 eruptions after 1960. Hatching displays areas at or over 95% Significance using a two tailed t-test.

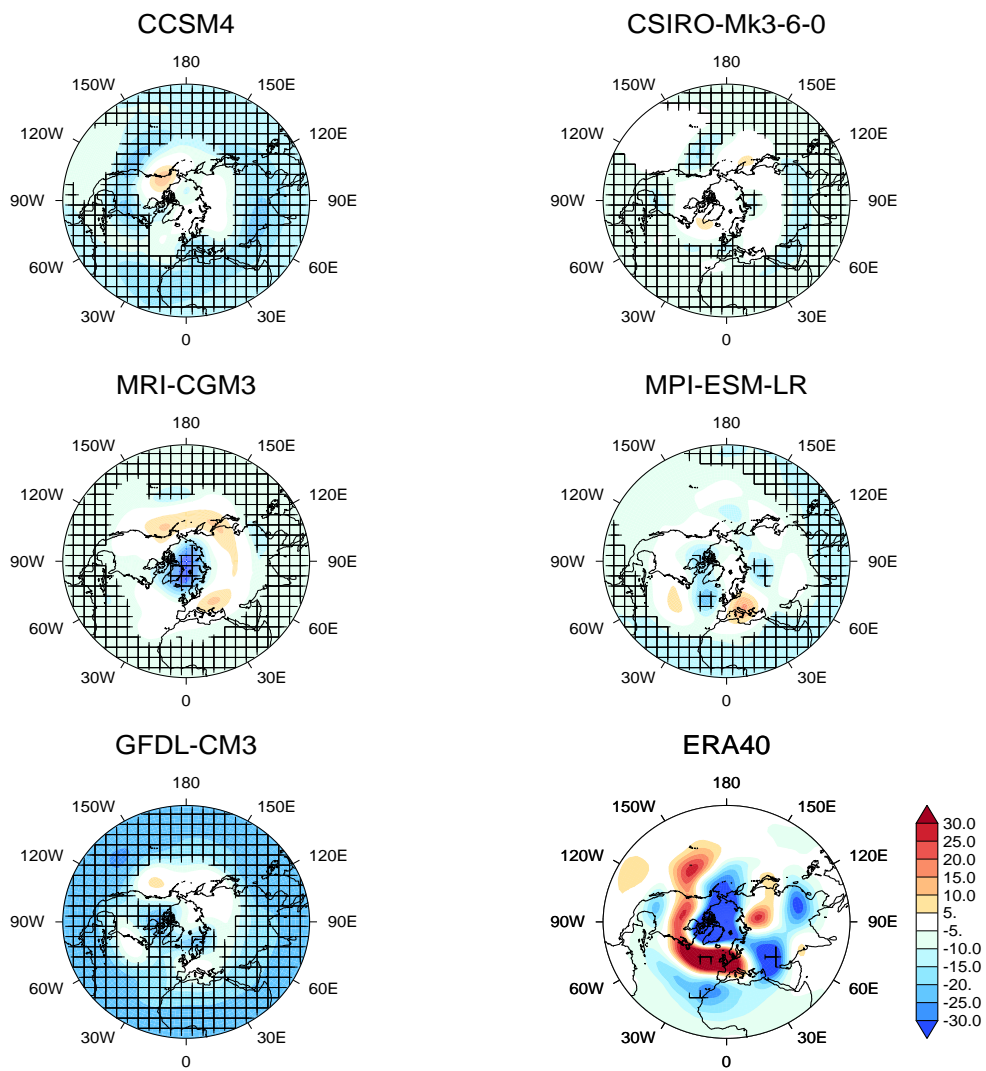


Figure 4.8: (continued)

Figure 4.9: IMAGE LEFT BLANK TO REDUCE PDF SIZE. NH stereographic plot of composite 50 hPa Geopotential Height anomalies (m) for the two following winters of the past nine most recent large tropical volcanic eruptions in all models and ERA40 reanalysis. The anomalies in the reanalysis are computed for the 4 eruptions after 1960. Hatching displays areas at or over 95% Significance using a two tailed t-test.

Figure 4.9: IMAGE LEFT BLANK TO REDUCE PDF SIZE. (**continued**)

As with temperature and MSLP, the difference in the anomalies of 50 hPa and 200 hPa geopotential height between the multi-model mean and the observations, Fig. ??c,d, is highly significant and confirms the difficulty of models to simulate the observed circulation changes in the stratosphere and upper-troposphere.

4.0.4.4 NAO index

As noted in section 3.2, the observed anomalies in the MSLP in the post-volcanic winters are not well reproduced by the CMIP5 models. The observed MSLP anomalies in the winters after the largest volcanic eruptions since 1880, project onto the leading variability mode of the NH circulation, especially the NAO index, with a significant prevalence of positive NAO in the first winter after the eruption (?), both in terms of amplitude and number of positive events (?).

In this section we test whether looking at the principal modes of variability can help to better isolate the dynamic response in the model simulations. As mentioned in section 2, we use the same time convention adopted by ? and S06 to identify the 1st and 2nd winter after each eruption. The majority of the volcanoes erupted in the spring-early summer but two erupted in autumn, the minor eruption of Fuego in October 1974 and the large eruption of Santa María at the end of October 1902. It is likely that their full effect won't be present in the first winter immediately after the eruption and therefore the first winter should be considered to be a full year after the eruption time, as listed in our Table ???. This differs from the time convention adopted by ? who considered the first winter immediately after the eruption for all the volcanoes, hence changing the years of winters considered for the two eruptions of Fuego and Santa María. In his paper he reported the robustness of his results when those two eruptions are excluded from the analysis. However, we show here that with the different dating convention the results are affected when these two eruptions are included.

When all nine eruptions south of 40°N as listed in Table ??? are included, the 20CRv2 shows a clear prevalence of positive NAO index in the first year after the eruptions (Fig. ??, 20CRv2, lag 0). The amplitude is significant roughly at the 4% level with seven volcanoes out of nine with positive NAO in the first winter and this occurrence is significant at the 9% level. No significant signals are observed for the second post-volcanic winter.

Only two post-volcanic winters show a negative NAO, after the eruptions of Agung and Quizapu, which both erupted in the southern hemisphere. Agung's aerosol was mostly concentrated south of the Equator (?) and Quizapu has the weakest effect on

the stratospheric optical depth and temperature between 30°S and 30°N among all the analyzed volcanoes (Figs. ?? and ??). This could affect the dynamics associated with the forcing of the NAO circulation. Our results are unchanged if we exclude the Quizapu eruption from the volcanoes used in the composite. We also note that, although positive, the winter 1903-04 after the Santa María eruption has a NAO signal close to zero (0.03, also consistent in the DJFM composite with -0.04 as confirmed in ?, his Fig. 2), which further reduces the number of occurrences of positive NAO events in the first winter after an eruption.

Figure 4.10: IMAGE LEFT BLANK TO REDUCE PDF SIZE. Superposed epoch analysis for the winter (DJF) NAO index for the 13 CMIP5 models and the 20th century reanalysis (20CRv2) for the 9 eruptions listed in Table ???. The average over 9 volcanic eruptions is shown at different lag time. Lag 0 indicates the first winter after a volcanic eruption. The horizontal lines show, from bottom to top, the 1st, 5th, 95th and 99th percentiles of the bootstrap distribution. For each plot is indicated the number of ensemble members (r), the ratio of total number of winters with positive NAO with respect to the total number of winters in each ensemble (σ) and the number of winters at lag 0 with positive NAO (N_0) with the relative p-value.

Figure 4.10: IMAGE LEFT BLANK TO REDUCE PDF SIZE. (**continued**)

Figure 4.11: IMAGE LEFT BLANK TO REDUCE PDF SIZE. As Fig ?? but using the convention adopted in ? for the first winter after the eruptions of Santa María (1902-1903) and Fuego (1974-1975).

Figure 4.11: IMAGE LEFT BLANK TO REDUCE PDF SIZE. (**continued**)

Among the 13 models analysed in this study, positive NAO signal at lag 0 is observed only for GISS-E2-R (at the 7% significance level) and CanESM2 at the 3% significance level. Only CNRM-CM5 shows a significant number of positive NAO events at lag 0 (52/90, $p=0.07$) but the composite amplitude reaches only 11% of significance level. The analysis is confirmed by the MSLP gridded anomalies shown in Fig. ?? where CanESM2 also shows a weak NAO-like dipole when averaged across 2 winter seasons. The MRI-CGM3 is the only model that shows a significant number of positive NAO events in the second winter after the eruptions ($p=0.08$) but the model appears to have a positive NAO at all lag times, so it is not clear whether this response is necessarily associated with the volcanic eruption.

The other models show no significant positive anomaly at lag 0, but many spurious signals are detected at various lags for different models. CSIRO-Mk3.6 displays a negative NAO at lag 0, while other models (NorESM1-M and CCSM4) show negative NAO at lag-1. HadCM3 and CNRM-CM5 detect a positive NAO at lag -3: the signal could partially be due to the degenerate contribution of the Krakatau eruptions that happens 3 years before the 1886 eruption of Tarawera and shows a positive NAO in both of these models (not shown). Finally, strong signals are displayed by HadGEM2-ES at lag -1 and NorESM1-M at lag +1: such signals could both be unphysical and occur by chance or they could also depend on periodicity sampled in the epoch analysis at the same frequency of the volcanic signal. We have not analyzed in detail the origin of the spurious result of these two models.

As mentioned above, when a different convention is used to identify the closest winters affected by the eruption of Santa María and Fuego, changes are observed in the superposed epoch analysis. Figure ?? examines the robustness of the analysis with respect to the choice of the winters after Santa María and Fuego, using the convention adopted in ?. Since the reanalysis are based on a limited sample, they prove to be highly sensitive to changes in the epoch key date. The signal at lag 0 becomes now highly significant (1% level) with an occurrence of 7 positive NAO out of 9 events ($p=0.09$). Most of the change in the signal comes from the Santa María event, which shows a strong positive NAO in the winter 1902-1903, immediately after the eruption and positively contributes to enhance the epoch composite at lag 0.

The largest effect of the change of the year of the first winter after the eruptions of Santa María and Fuego is observed for HadGEM2, which does not detect any significant signal at any lag. With 10 ensemble members, CNRM-CM5 is the only one that still detects a positive NAO at lag 0. The amplitude is small but slightly more significant than in the previous composite (it reaches now the 10% level of significance) and the number of events is significant (56/90, $p=0.02$). Among the other models, only MRI-CGM3 detects a significant number of positive events at lag 0 (18/27, $p=0.08$) but, as noted before, the models tends to show positive NAO almost at all lags. Although this model shows the strongest decrease of the geopotential height at high latitudes both at 50 hPa and 200 hPa, this seems not enough to reproduce a significant NAO signal or surface temperature anomaly.

The main conclusions of this section are 1) the superposed epoch analysis of the 20CRv2 NAO index confirms previous findings of a positive NAO in the first winter following the major tropical eruptions in the 19th and 20th century, but the strength of the signal is sensitive to the choice of the key dates for each eruption, which points to the sparseness of observations hampering our understanding of processes. 2) as observed in the previous sections, the models struggle to reproduce a detectable positive NAO signal in the first post-eruption winter. With 10 ensemble members, the CNRM-CM5 model results are the most robust to changes in the definition of the post-volcanic key dates. With less ensemble members, the other models show sensitivity to the definition of the key dates. We finally note that, since in this work we only analyzed the ensemble of CMIP5 historical runs, the bootstrap distribution might give a conservative estimate of the significance associated with the signal. Clearer signal detection could be achieved by drawing the random matrix from the CMIP5 control simulations, therefore relying only on natural variability not influenced by volcanoes or other forcings.

4.0.5 Discussion and Conclusions

All available models submitted to the CMIP5 archive as of April 2012 that had a reasonably realistic representation of volcanic eruptions and number of samples have been analyzed for their ability to simulate post-volcanic radiative and dynamic responses. With substantially different dynamics between the models it was hoped to find at least one model simulation that was dynamically consistent with observations, showing improvement since S06. Disappointingly, we found that again, as with S06, despite relatively consistent post volcanic radiative changes, none of the models manage to simulate a sufficiently strong dynamical response. Although all the models reproduce reasonably well the increase in geopotential height in the lower stratosphere at low latitudes, none of the models simulate a sufficiently strong reduction in the geopotential height at high latitudes and correspondingly the MSLP pressure fields and temperature fields show major differences with respect to the observed anomalies. This is despite some models having 10 ensemble members, giving a potentially strong signal to noise ratio.

It is unclear why models fail to simulate the dynamics following volcanic eruptions. The dynamical mechanism proposed by ? (their Fig. 13), involves lower stratosphere tropical heating caused by the presence of volcanic aerosols which gives rise to a stronger polar vortex due to the thermal wind relationship. A stronger vortex also could be due to a decrease in planetary wave forcing from the troposphere, although the evidence for this is unclear. The modelling results of ? showed a decreased EP flux into the stratosphere following the Pinatubo eruption but observations suggest an increase in the EP flux following the Agung, Fuego, El Chichón and Pinatubo eruptions (?). S06 suggested that models might be biased towards an unrealistically strong polar vortex which results in a weak wave feedback between stratosphere and troposphere. From column three of Table ?? we observe a large variability among the 13 models in their climatological 50 hPa zonal wind at high latitude. Some models have stronger zonal winds compared to ERA40 but their response to volcanic forcing does not differ from what is observed for the models characterized by a lower climatological wind. Although this does not confirm the findings of S06, based on a limited number of models, we also notice that all models show considerably less variability

in high-latitude stratospheric winds than observed, suggesting a stable polar vortex and more resistance to changes from external forcings, as found by S06.

Table 4.3: Climatological indices

Model Name	U50hPa 30°S-30°N m/s	U50hPa 55°N-65°N m/s	ENSO 3.4 Index
bcc-csm1.1	-5.9(0.5)	27.4(2.5)	-0.06
HadGEM2-ES	-5.7(0.5)	24.1(2.2)	-0.12
HadCM3	-3.1(0.3)	14.7(1.0)	-0.11
CNRM-CM5	-5.0(0.2)	17.6(1.0)	-0.22
GISS-E2-H	-3.1(0.5)	13.0(1.3)	-0.67
GISS-E2-R	-2.7(0.6)	13.8(2.0)	-0.33
NorESM1-M	-7.9(0.8)	20.2(2.1)	-0.06
CCSM4	-8.2(0.7)	25.1(2.4)	-0.12*
CSIRO-Mk3-6-0	-0.7(0.3)	8.7(0.3)	-0.11**
MRI-CGCM3	-3.3(0.4)	25.2(2.9)	-0.10
MPI-ESM-LR	-8.4(0.5)	17.9(2.5)	-0.15
GFDL-CM3	-9.0(0.6)	24.2(1.8)	-0.33
Reanalysis	-3.7(5.0)	19.4(5.4)	0.07

U50hPa is the winter (DJF) seasonal climatological zonal wind computed for two regions, 30°S-30°N and 55°N-65°N. In bracket is the standard deviation. The last column shows the ENSO 3.4 index (see text). In the last row the climatological wind from ERA40 and the ENSO 3.4 index from 20CRv2 based on HadISST.

*with 5 ensembles **with 8 ensembles

There are therefore still uncertainties in the dynamical mechanisms following volcanic eruptions particularly regarding the wave propagation through the polar stratosphere as seen in EP flux diagnostics (?).

In addition, the degree of El Niño influence and interaction following volcanic eruptions is unknown. Based on the superposed epoch analysis of post-volcanic winters stratified according to the ENSO phase, ? concluded that the ENSO does not change the impact of volcanic eruptions on the Northern Hemisphere winter circulation, although the low number of cases imposes caveats on the conclusions. A recent work (?) argues that ENSO has a different effect on the Northern Hemispheric winter circulation when the differences between Central-Pacific (CP) and East-Pacific (EP) El Niño events are taken into account. In particular, CP El Niño events appear to have a significant effect on winter NH circulation, with a tendency towards a negative NAO index. According to their definition, CP El Niño occurred in 1963-1964 and 1991-1992 but not in 1982-1983, which could explain the strong Eurasian warming signal observed after El Chichón, even though a strong El Niño event was taking place, and the relatively disturbed vortex in January 1992 (?). Moreover, biases in model representations of ENSO variability (?) could in the same way affect their response to volcanic forcing. The issue is also complicated by the intrinsic problems in defining the modes of ENSO variability (?). In our analysis the large number of ensemble members should help to smooth out possible contaminations induced by the Pacific SST variability. Despite this, the models have a tendency to be in small negative ENSO phase, indicative of a weak La Niña phase. However, this should not lead to a weakening of the volcanic response in the models. Whilst Manzini et al. (2006) saw in model simulations that during the El Niño phase there was an increase in the vertical propagation of quasi-stationary planetary waves into the stratosphere from the troposphere, which caused a weaker, more disturbed vortex, during the La Niña phase they noticed no influence distinguishable from variability. Further studies using observations and model data have concluded similar results (??). Despite the model performance, the 20CRv2 reanalysis dataset, which uses HadISST sea surface temperatures, yields an averaged ENSO 3.4 index of 0.07 during the volcanic eruptions analyzed here. It has also been suggested that large volcanic eruptions could actually

trigger a positive phase of ENSO. ? performed linear regressions on the HadISST and the Extended Reconstructed SST (ERSST) dataset. Whilst finding a weakly negative temperature volcanic response from linear regressions of the HadISST and the ERSST datasets using the ST dataset as the volcanic signal, if the cold tongue index is assumed not independent of volcanoes in their linear regression, they find a large positive ENSO like pattern. Their findings, independent of the choice of volcano index, suggests a statistically significant El Niño response to a volcanic eruption in observations.

Whilst uncertainty still remains on the interactions between volcanoes and ENSO, the DJF warming signal can be seen independent of the choice of volcanoes, with the choice of the last four major eruptions, the last nine as used here, or longer term reconstructions of temperature from 1600 (?) and the past half millenium (?) which all reveal a statistically significant DJF warming following major volcanic eruptions, which, as noted by (?), is extremely unlikely to be an artifact of internal variability. Despite this, we performed calculations of the DJF temperature anomaly for also the five biggest volcanoes (Krakatau, Santa María, Agung, El Chichón and Pinatubo) and also for the four best observed volcanoes that erupted in the satellite era (Agung, Fuego, El Chichón and Pinatubo) for all the models and the observations. Despite the observations showing, independent of these choices, a strong statistically significant warming, none of the models successfully simulate the observed response. GISS-E2-H shows a slightly increased DJF warming pattern, yet further investigation of MSLP anomalies reveal neither a large nor anywhere statistically significant positive NAO. bcc-csm1.1 also shows a small increase in surface temperature over the Eurasian region, yet the spatial response is not correct. Moreover, there is almost no statistical significance in the bcc-csm1.1 temperature fields over the Eurasian region and further investigation in this model reveals neither a positive or significant NAO signal.

Finally, ? found that including the Quasi-Biennial Oscillation (QBO) in the model made a substantial difference to the volcanic impact on the vortex. They found in observations following the Pinatubo eruption that the vortex was strengthened more in the second winter than the first, despite more aerosol being present in the stratosphere in the first winter. They proposed that this could be explained by the

QBO being in the East phase in the first winter, which tends to weaken the vortex, and was in the West phase in the second winter, which tends to strengthen it. They concluded that a model with a QBO in the correct phase could better represent the dynamical simulation of the Pinatubo eruption. We note here that none of the models tested have a QBO in them, as can be observed from Table ?? by the low standard deviation in the climatological winter 50 hPa zonal wind over the equator, which could affect the performance of the dynamical simulation.

Another factor which could account for the poor simulation of the dynamical response following a volcanic eruption is related to how the aerosol is imposed in the model. We note that it is typical for a model to employ a very crude representation of aerosol in four latitude bands (?), and the question of the suitability of this aerosol representation has been raised before (??). Another reason for the “common failure” of models to simulate the dynamics following volcanic eruptions may be their representation of the AO. ? notes that it may be that models have a general basic inadequacy that does not allow a sufficiently strong AO response to large-scale forcing. Others have pointed to ozone as being an important factor (??), however, as noted by ? the response to the past major eruptions (before major ozone loss and larger amounts of ozone destroying chlorine in the atmosphere) is similar to that of El Chichón and Pinatubo combined, which suggests that inclusion of ozone chemistry is unlikely to be a major factor in the simulation of a volcanic eruption.

The impact of volcanic eruptions on surface climate is the closest natural analogue to sulfate aerosol geoengineering, despite the differences in injection method and duration of the perturbation. Unlike sulfate aerosol geoengineering, the ability of models to accurately reproduce the response to volcanic eruptions can be tested against observations. Despite it being likely that a more uniform profile of aerosol in the stratosphere would occur from geoengineering than following volcanic eruptions, the results of GCM simulations of stratospheric geoengineering need to be considered in the light of their limitations when it comes to certain aspects of their responses to volcanic eruptions. This is of concern not only for the temperature response, but also for the precipitation response, as the dynamical effects following an eruption can often overwhelm the radiative response (?). Accordingly, research into the climate

response to volcanic eruptions and their simulations is an area of major importance, not only in its own right, but for stratospheric aerosol geoengineering.

Bibliography

- Adams, B. J., M. E. Mann, and C. M. Ammann (2003), Proxy evidence for an El Niño-like response to volcanic forcing, *Nature*, *426*(6964), 274–278.
- Ammann, C. M., G. A. Meehl, W. M. Washington, and C. S. Zender (2003), A monthly and latitudinally varying volcanic forcing dataset in simulations of 20th century climate, *Geophys. Res. Lett.*, *30*, 1657, doi:10.1029/2003GL016,875.
- Ammann, C. M., F. Joos, D.S. Schimel, B.L. Otto-Bliesner, and R.A. Tomas (2007), Solar influence on climate during the past millennium Results from transient simulations with the NCAR Climate System Model, *Proceedings of the National Academy of Sciences of the United States*, *104*, 3713-3718.
- Anchukaitis, K. J., B. M. Buckley, E. R. Cook, B. I. Cook, R. D. D’Arrigo, and C. M. Ammann (2010), Influence of volcanic eruptions on the climate of the asian monsoon region, *Geophys. Res. Lett.*, *37*(22), doi:10.1029/2010GL044843.
- Andres, R. J., and A. D. Kasgnoc (1998), A time-averaged inventory of sub-aerial volcanic sulfur emissions, *J. Geophys. Res.*, *103*(D19), 25,251–25,261, doi:10.1029/98JD02091.
- Andrews, D., J. Holton, and C. Leovy (1987), *Middle Atmosphere Dynamics*, Academic Pr, Orlando, Fla.
- Andronova, N. G., E. V. Rozanov, F. Yang, M. E. Schlesinger, and G. L. Stenchikov (1999), Radiative forcing by volcanic aerosols from 1850 to 1994, *J. Geophys. Res.*, *104*(D14), 16,807–16,826, doi:10.1029/1999JD900165.

- Baldwin, M. P., and T. J. Dunkerton (1999), Propagation of the Arctic Oscillation from the stratosphere to the troposphere, *J. Geophys. Res.*, *104*(D24), 30,937–30,946, doi:10.1029/1999JD900445.
- Baldwin, M. P., and T. J. Dunkerton (2001), Stratospheric harbingers of anomalous weather regimes, *Science*, *294*(5542), 581–584, doi:10.1126/science.1063315.
- Baran, A. J., and J. S. Foot (1994), New application of the operational sounder hirs in determining a climatology of sulphuric acid aerosol from the pinatubo eruption, *J. Geophys. Res.*, *99*(D12), 25,673–25,679, doi:10.1029/94JD02044.
- Barnes, J. E., and D. J. Hofmann (1997), Lidar measurements of stratospheric aerosol over mauna loa observatory, *Geophys. Res. Lett.*, *24*(15), 1923–1926, doi:10.1029/97GL01943.
- Black, R. X. (2002), Stratospheric Forcing of Surface Climate in the Arctic Oscillation, *Journal of Climate*, *15*(3), 268–277, doi:10.1175/1520-0442(2002)015.
- Bluth, G. J. S., W. I. Rose, I. E. Sprod, and A. J. Krueger (1997), Stratospheric loading of sulfur from explosive volcanic eruptions, *J. of Geology*, *105*(6), 671–684.
- Calvo, N., M. A. Giorgetta, R. Garcia-Herrera, and E. Manzini (2009), Nonlinearity of the combined warm ENSO and QBO effects on the Northern Hemisphere polar vortex in MAECHAM5 simulations, *J. Geophys. Res.*, *114*(D13), doi:10.1029/2008JD011445.
- Christiansen, B. (2008), Volcanic Eruptions, Large-Scale Modes in the Northern Hemisphere, and the El Niño - Southern Oscillation, *J. Clim.*, *21*, 910–922.
- Chylek, P., J. Li, M. K. Dubey, M. Wang, and G. Lesins (2011), Observed and model simulated 20th Century Arctic temperature variability: Canadian Earth System Model CanESM2, *Atmospheric Chemistry and Physics Discussions*, *11*(8), 22,893–22,907, doi:10.5194/acpd-11-22893-2011.

- Collins, M., S. F. B. Tett, and C. Cooper (2001), The internal climate variability of HadCM3, a version of the Hadley Centre coupled model without flux adjustments, *Climate Dynamics*, *17*, 61–81, 10.1007/s003820000094.
- Collins, W. J., et al. (2011), Development and evaluation of an Earth-System model - HadGEM2, *Geoscientific Model Development*, *4*(4), 1051–1075, doi:10.5194/gmd-4-1051-2011.
- Compo, G. P., et al. (2011), The twentieth century reanalysis project, *Q. J. R. Meteorol. Soc.*, *137*(654), 1–28, doi:10.1002/qj.776.
- Delworth, T. L., and K. W. Dixon (2000), Implications of the Recent Trend in the Arctic/North Atlantic Oscillation for the North Atlantic Thermohaline Circulation, *Journal of Climate*, *13*(21), 3721–3727, doi:10.1175/1520-0442(2000)013.
- Donner, L. J., et al. (2011), The Dynamical Core, Physical Parameterizations, and Basic Simulation Characteristics of the Atmospheric Component AM3 of the GFDL Global Coupled Model CM3, *Journal of Climate*, *24*(13), 3484–3519, doi:10.1175/2011JCLI3955.1.
- Efron, B., and R. Tibshirani (1986), Bootstrap methods for standard errors, confidence intervals, and other measures of statistical accuracy., *Stat Sci*, *1*, 54–75.
- Fischer, E. M., J. Luterbacher, E. Zorita, S. F. B. Tett, C. Casty, and H. Wanner (2007), European climate response to tropical volcanic eruptions over the last half millennium, *Geophys. Res. Lett.*, *34*(5), doi:10.1029/2006GL027992.
- Forster, P., et al. (2007), Changes in atmospheric constituents and in radiative forcing, in *Climate Change 2007: The Physical Science Basis. Contribution of Working Group I to the Fourth Assessment Report of the Intergovernmental Panel on Climate Change*, edited by S. Solomon, D. Qin, M. Manning, Z. Chen, M. Marquis, K. Averyt, M. Tignor, and H. Miller, ISBN 978-0-521-88009-1 (pb: 978-0-521-70596-7), Cambridge University Press, Cambridge, United Kingdom and New York, NY, USA.

- Garcia-Herrera, R., N. Calvo, R. R. Garcia, and M. A. Giorgetta (2006), Propagation of ENSO temperature signals into the middle atmosphere: A comparison of two general circulation models and ERA-40 reanalysis data, *J. Geophys. Res.*, *111*(D6), doi:10.1029/2005JD006061.
- Gent, P. R., et al. (2011), The Community Climate System Model Version 4, *Journal of Climate*, *24*(19), 4973–4991, doi:10.1175/2011JCLI4083.1.
- Graf, H.-F., and D. Zanchettin (2012), Central Pacific El Niño, the “sub-tropical bridge” and Eurasian climate, *J. Geophys. Res.*, *117*(D1), doi:10.1029/2011JD016493.
- Graf, H.-F., Q. Li, and M. A. Giorgetta (2007), Volcanic effects on climate: revisiting the mechanisms, *Atmospheric Chemistry and Physics*, *7*(17), 4503–4511, doi:10.5194/acp-7-4503-2007.
- Guilyardi, E. (2006), El Niño–mean state–seasonal cycle interactions in a multi-model ensemble, *Climate Dynamics*, *26*, 329–348, 10.1007/s00382-005-0084-6.
- Hess, M., P. Koepke, and I. Schult (1998), Optical Properties of Aerosols and Clouds: The software package OPAC, *Bull. Am. Met. Soc.*, *79*, 831–844.
- Hurrell, J. W., and C. Deser (2009), North Atlantic climate variability: The role of the North Atlantic Oscillation, *Journal of Marine Systems*, *78*(1), 28 – 41, doi:10.1016/j.jmarsys.2008.11.026.
- IPCC Core Writing Team, R. Pachauri, and A. Reisinger (Eds.) (2007), *Climate Change 2007: Synthesis Report. Contribution of Working Groups I, II and III to the Fourth Assessment Report of the Intergovernmental Panel on Climate Change*, Cambridge Univ. Press, 104 pp.
- Kirkevåg, A., T. Iversen, Ø. Seland, J. B. Debernard, T. Storelvmo, and J. E. Kristjansson (2008), Aerosol-cloud-climate interactions in the climate model cam-oslo, *Tellus A*, *60*(3), 492–512, doi:10.1111/j.1600-0870.2008.00313.x.

- Kirkevåg, A., T. Iversen, Ø. Seland, C. Hoose, J. E. Kristjánsson, H. Struthers, A. Ekman, S. Ghan, J. Griesfeller, D. Nilsson and M. Schulz (2012), Aerosol-climate interactions in the Norwegian Earth System Model - NorESM, *To be submitted to GMD*
- Kistler, R., et al. (2001), The NCEP–NCAR 50–Year Reanalysis: Monthly Means CD–ROM and Documentation, *Bulletin of the American Meteorological Society*, *82*(2), 247–267, doi:10.1175/1520-0477(2001)082.
- Kolstad, E., and A. Charlton-Perez (2010), Observed and simulated precursors of stratospheric polar vortex anomalies in the Northern Hemisphere, *Climate Dynamics*, *37*(7), 1443–1456.
- Kravitz, B., and A. Robock (2011), Climate effects of high-latitude volcanic eruptions: Role of the time of year, *J. Geophys. Res.*, *116*(D1), doi:10.1029/2010JD014448.
- Lambert, A., R. G. Grainger, J. J. Remedios, C. D. Rodgers, M. Corney, and F. W. Taylor (1993), Measurements of the evolution of the Mt. Pinatubo aerosol cloud by ISAMS, *Geophys. Res. Lett.*, *20*(12), 1287–1290, doi:10.1029/93GL00827.
- Manzini, E., M. A. Giorgetta, M. Esch, L. Kornblueh, and E. Roeckner (2006), The Influence of Sea Surface Temperatures on the Northern Winter Stratosphere: Ensemble Simulations with the MAECHAM5 Model, *Journal of Climate*, *19*(16), 3863–3881, doi:10.1175/JCLI3826.1.
- Marshall, A. G., A. A. Scaife, and S. Ineson (2009), Enhanced seasonal prediction of european winter warming following volcanic eruptions, *Journal of Climate*, *22*(23), 6168–6180, doi:10.1175/2009JCLI3145.1.
- Marsland, S., H. Haak, J. Jungclaus, M. Latif, and F. Roeske (2003), The Max-Planck-Institute global ocean/sea ice model with orthogonal curvilinear coordinates., *Ocean Modell.*, *5*, 91–127.
- Meehl, G., C. Covey, T. Delworth, M. Latif, B. McAvaney, J. Mitchell, R. Stouffer, and K. Taylor (2007), The WCRP CMIP3 multi-model dataset: a new era in

- climate change research, *Bulletin of the American Meteorological Society*, *88*, 1383–1394.
- Mitchell, D., L. Gray, J. Anstey, M. Baldwin, and J. Charlton-Perez (2012), The influence of Stratospheric Vortex Displacements and Splits on Surface Climate, *J. Clim. in revision*.
- Mitchell, D. M., L. J. Gray, and A. J. Charlton-Perez (2011), The structure and evolution of the stratospheric vortex in response to natural forcings, *J. Geophys. Res.*, *116*(D15), doi:10.1029/2011JD015788.
- Mizuta, R., et al. (2012), Climate simulations using MRI-AGCM3.2 with 20-km grid, *J. Meteor. Soc. Japan*, *in press*.
- Oman, L., A. Robock, G. Stenchikov, G. A. Schmidt, and R. Ruedy (2005), Climatic response to high-latitude volcanic eruptions, *J. Geophys. Res.*, *110*(D13), doi:10.1029/2004JD005487.
- Otterå, O. (2008), Simulating the effects of the 1991 Mount Pinatubo volcanic eruption using the ARPEGE atmosphere general circulation model, *Advances in Atmospheric Sciences*, *25*, 213–226, 10.1007/s00376-008-0213-3.
- Raddatz, T., C. Reick, W. Knorr, J. Kattge, E. Roeckner, R. Schnur, K.-G. Schnitzler, P. Wetzell, and J. Jungclaus (2007), Will the tropical land biosphere dominate the climate–carbon cycle feedback during the twenty-first century?, *Climate Dynamics*, *29*, 565–574, 10.1007/s00382-007-0247-8.
- Ramachandran, S., V. Ramaswamy, G. L. Stenchikov, and A. Robock (2000), Radiative impact of the Mount Pinatubo volcanic eruption: Lower stratospheric response, *J. Geophys. Res.*, *105*(D19), 24,409–24,429.
- Rasch, P. J., S. Tilmes, R. P. Turco, A. Robock, L. Oman, C.-C. J. Chen, G. L. Stenchikov, and R. R. Garcia (2008), An overview of geoengineering of climate using stratospheric sulphate aerosols, *Philosophical Transactions of the Royal Society A: Mathematical, Physical and Engineering Sciences*, *366*(1882), 4007–4037, doi:10.1098/rsta.2008.0131.

- Robock, A. (2000), Volcanic eruptions and climate, *Rev. Geophys.*, *38*(2), 191–219.
- Robock, A., and J. Mao (1992), Winter warming from large volcanic eruptions, *Geophys. Res. Lett.*, *19*(24), 2405–2408, doi:10.1029/92GL02627.
- Robock, A., and J. Mao (1995), The volcanic signal in surface temperature observations, *J. Clim.*, *8*, 1086–1103.
- Rodwell, M. J., D. P. Rowell, and C. K. Folland (1999), Oceanic forcing of the winter-time North Atlantic Oscillation and European climate, *Nature*, *398*(6725), 320–323.
- Rotstayn, L. D., M. A. Collier, M. R. Dix, Y. Feng, H. B. Gordon, S. P. O’Farrell, I. N. Smith, and J. Syktus (2010), Improved simulation of australian climate and enso-related rainfall variability in a global climate model with an interactive aerosol treatment, *International Journal of Climatology*, *30*(7), 1067–1088, doi:10.1002/joc.1952.
- Sato, M., J. Hansen, M. McCormick, and J. Pollack (1993), Stratospheric aerosol optical depths, *J. Geophys. Res.*, *98*, 22,987–22,994, doi:10.1029/93JD02,553.
- Schmidt, G. A., et al. (2006), Present-Day Atmospheric Simulations Using GISS ModelE: Comparison to In Situ, Satellite, and Reanalysis Data, *Journal of Climate*, *19*(2), 153–192, doi:10.1175/JCLI3612.1.
- Shindell, D. T., G. A. Schmidt, M. E. Mann, and G. Faluvegi (2004), Dynamic winter climate response to large tropical volcanic eruptions since 1600, *J. Geophys. Res.*, *109*(D5), doi:10.1029/2003JD004151.
- Stenchikov, G., A. Robock, V. Ramaswamy, M. D. Schwarzkopf, K. Hamilton, and S. Ramachandran (2002), Arctic Oscillation response to the 1991 Mount Pinatubo eruption: Effects of volcanic aerosols and ozone depletion, *J. Geophys. Res.*, *107*(D24), doi:10.1029/2002JD002090.
- Stenchikov, G., K. Hamilton, A. Robock, V. Ramaswamy, and M. D. Schwarzkopf (2004), Arctic oscillation response to the 1991 Pinatubo eruption in the SKYHI

- general circulation model with a realistic quasi-biennial oscillation, *J. Geophys. Res.*, *109*(D3), doi:10.1029/2003JD003699.
- Stenchikov, G., K. Hamilton, R. J. Stouffer, A. Robock, V. Ramaswamy, B. Santer, and H.-F. Graf (2006), Arctic Oscillation response to volcanic eruptions in the IPCC AR4 climate models, *J. Geophys. Res.*, *111*(D7), doi:10.1029/2005JD006286.
- Stenchikov, G., T. L. Delworth, V. Ramaswamy, R. J. Stouffer, A. Wittenberg, and F. Zeng (2009), Volcanic signals in oceans, *J. Geophys. Res.*, *114*(D16), doi:10.1029/2008JD011673.
- Stenchikov, G. L., I. Kirchner, A. Robock, H.-F. Graf, J. C. Antuña, R. G. Grainger, A. Lambert, and L. Thomason (1998), Radiative forcing from the 1991 mount pinatubo volcanic eruption, *J. Geophys. Res.*, *103*(D12), 13,837–13,857, doi:10.1029/98JD00693.
- Stothers, R. B. (1996), Major optical depth perturbations to the stratosphere from volcanic eruptions: Pyrheliometric period, 1881 1960, *J. Geophys. Res.*, *101*(D2), 3901–3920, doi:10.1029/95JD03237.
- Stothers, R. B. (2001), Major optical depth perturbations to the stratosphere from volcanic eruptions: Stellar extinction period, 1961 1978, *J. Geophys. Res.*, *106*(D3), 2993–3003, doi:10.1029/2000JD900652.
- Takahashi, K., A. Montecinos, K. Goubanova, and B. Dewitte (2011), ENSO regimes: Reinterpreting the canonical and Modoki El Niño, *Geophys. Res. Lett.*, *38*(10), doi:10.1029/2011GL047364.
- Tanaka, T. Y., K. Orito, T. T. Sekiyama, K. Shibata, M. Chiba, and H. Tanaka (2003), MASINGAR, a global tropospheric aerosol chemical transport model coupled with MRI/JMA98 GCM: Model description, *Meteor. Geophys.*, *53*(4), 119–138.
- Taylor, K. E., R. J. Stouffer, and G. A. Meehl (2011), An Overview of CMIP5 and the Experiment Design, *Bull. Am. Met. Soc.*, *93*(4), 485–498, doi:10.1175/BAMS-D-11-00094.1.

- Thompson, D. W. J., and J. M. Wallace (1998), The Arctic oscillation signature in the wintertime geopotential height and temperature fields, *Geophys. Res. Lett.*, *25*(9), 1297–1300, doi:10.1029/98GL00950.
- Thompson, D. W. J., and J. M. Wallace (2001), Regional Climate Impacts of the Northern Hemisphere Annular Mode, *Science*, *293*(5527), 85–89, doi:10.1126/science.1058958.
- Thompson, D. W. J., M. P. Baldwin, and J. M. Wallace (2002), Stratospheric Connection to Northern Hemisphere Wintertime Weather: Implications for Prediction, *Journal of Climate*, *15*(12), 1421–1428, doi:10.1175/1520-0442(2002)015.
- Timmreck, C., S. J. Lorenz, T. J. Crowley, S. Kinne, T. J. Raddatz, M. A. Thomas, and J. H. Jungclaus (2009), Limited temperature response to the very large AD 1258 volcanic eruption, *Geophys. Res. Lett.*, *36*(21), doi:10.1029/2009GL040083.
- Tung, K.-K., and J. Zhou (2010), The Pacific’s Response to Surface Heating in 130 Yr of SST: La Niña-like or El Niño-like?, *Journal of the Atmospheric Sciences*, *67*(8), 2649–2657, doi:10.1175/2010JAS3510.1.
- Uppala, S. M., et al. (2005), The ERA-40 re-analysis, *Quarterly Journal of the Royal Meteorological Society*, *131*(612), 2961–3012, doi:10.1256/qj.04.176.
- Voldoire, A., and coauthors (2011), The CNRM-CM5.1 global climate model: Description and basic evaluation, *technical doc*, CNRM-CM, available at <http://www.cnrn.meteo.fr/cmip5/>.
- Wu, T., R. Yu, and F. Zhang (2008), A modified dynamic framework for the atmospheric spectral model and its application, *Journal of the Atmospheric Sciences*, *65*(7), 2235–2253, doi:10.1175/2007JAS2514.1.
- Wu, T., et al. (2012), The 20th century global carbon cycle from the Beijing Climate Center Climate System Model (BCC_CSM), *J. Clim.*, *submitted*.

Yukimoto, S., and coauthors (2011), Meteorological Research Institute-Earth System Model v1 (MRI-ESM1) – Model Description, *Tech. Rep. Meteor. Res. Inst. 64*, 88pp., The Meteorological Research Institute.

Chapter 5

Simulations of volcanic eruptions using high-top and low-top configurations of HadGEM2

Left blank in this version, but it will include a description of the high-top and low-top version of HadGEM2-cc. It will include descriptions of the aerosol implementation, detailed descriptions of the experiments performed, and analysis of the results. (All the simulations that needed to be done for this section have been done, and a large part have been analysed and written up).

Chapter 6

Changing the prescription of aerosol in HadGEM2 high-top

Left blank in this version, but it will include a further description of the aerosol code in HadGEM2, the changes made in the code/model to the aerosol, and the resulting experiments. (Almost all experiments are done - others that need to be done have a run-time of about two weeks).

Chapter 7

Analysing the climatic response to sulphate aerosol geoengineering in a high-top model

Left blank in this version. Suggested chapter to analyse a small amount of the results that Scott Osprey is currently simulating. My involvement in the analysis has been proposed many times, but the specifics of what exactly I would include have not been agreed upon.

Chapter 8

Discussion, conclusions and further work

Left blank for this version, but a small number of examples of further work include:

- ITCZ changes and volcanic eruptions in the CMIP5 models - Sahelian drought
- SH dynamical response following volcanic eruptions in HadGEM2, CMIP5 and observations
- Brewer Dobson circulation changes following volcanic eruptions in HadGEM2
- Storm Track changes following volcanic eruptions
- Implementation of interactive aerosol for volcanic chemistry
- Sea Ice changes in the CMIP5 database and observation datasets following volcanic eruptions to aid the interpretation of geoengineering and sea ice studies

Appendix A

Appendix 1

Left blank in this version, but: EOFs - explanation of what they are, the theory behind them, how they can be used, with relevance to the CMIP5 section (not explained but referenced in my paper) and explanations of the epoch matrix (estimated about 5 pages).